6

Crystal Structures of Minerals in the Lower Mantle

June K. Wicks and Thomas S. Duffy

ABSTRACT

The crystal structures of lower mantle minerals are vital components for interpreting geophysical observations of Earth's deep interior and in understanding the history and composition of this complex and remote region. The expected minerals in the lower mantle have been inferred from high pressure-temperature experiments on mantle-relevant compositions augmented by theoretical studies and observations of inclusions in natural diamonds of deep origin. While bridgmanite, ferropericlase, and $CaSiO_3$ perovskite are expected to make up the bulk of the mineralogy in most of the lower mantle, other phases such as SiO_2 polymorphs or hydrous silicates and oxides may play an important subsidiary role or may be regionally important. Here we describe the crystal structure of the key minerals expected to be found in the deep mantle and discuss some examples of the relationship between structure and chemical and physical properties of these phases.

6.1. INTRODUCTION

Earth's lower mantle, which spans from 660 km depth to the core-mantle boundary (CMB), encompasses nearly three quarters of the mass of the bulk silicate Earth (crust and mantle). Our understanding of the mineralogy and associated crystal structures of this vast region has greatly expanded over the course of the past two decades with the development of new capabilities for reproducing in the laboratory the extreme pressures and temperatures expected to be found in the lower mantle (24–135 GPa and 1800–4000 K) [*Ricolleau et al.*, 2010; *Irifune and Tsuchiya*, 2015]. Most structural studies of lower mantle minerals have been carried out using the laser-heated diamond anvil cell with X-ray diffraction techniques, most commonly powder diffraction, as the primary diagnostic. Several recent review articles have summarized the major experimental methods for exploring the structures and properties of lower mantle minerals [*Duffy*, 2005; *Mao and Mao*, 2007; *Shen and Wang*, 2014; *Ito*, 2015].

The crystal structure is the most fundamental property of a mineral and is intimately related to its major physical and chemical characteristics, including compressibility, density, and sound velocities. As an example, observations of seismic anisotropy in the lowermost mantle are connected to the elastic anisotropy of the associated minerals, and this anisotropy is ultimately dictated by the mineral's chemical composition and the details of its crystal structure [*Karki et al.*, 1997b; *Marquardt et al.*, 2009; *Dobson et al.*, 2013]. Crystal structure also strongly influences the partitioning of elements between different phases and so plays an important role in the chemical state of the lower mantle as well.

The expected phase assemblages and the corresponding crystal structures are largely a function of the chemical makeup of the deep mantle. Figure 6.1 illustrates the expected mineralogies of the two major expected lithologies of the lower mantle. The pyrolite model, the most widely accepted model for the bulk lower mantle, is based

Department of Geosciences, Princeton University, Princeton, New Jersey, USA

Deep Earth: Physics and Chemistry of the Lower Mantle and Core, Geophysical Monograph 217, First Edition.
Edited by Hidenori Terasaki and Rebecca A. Fischer.

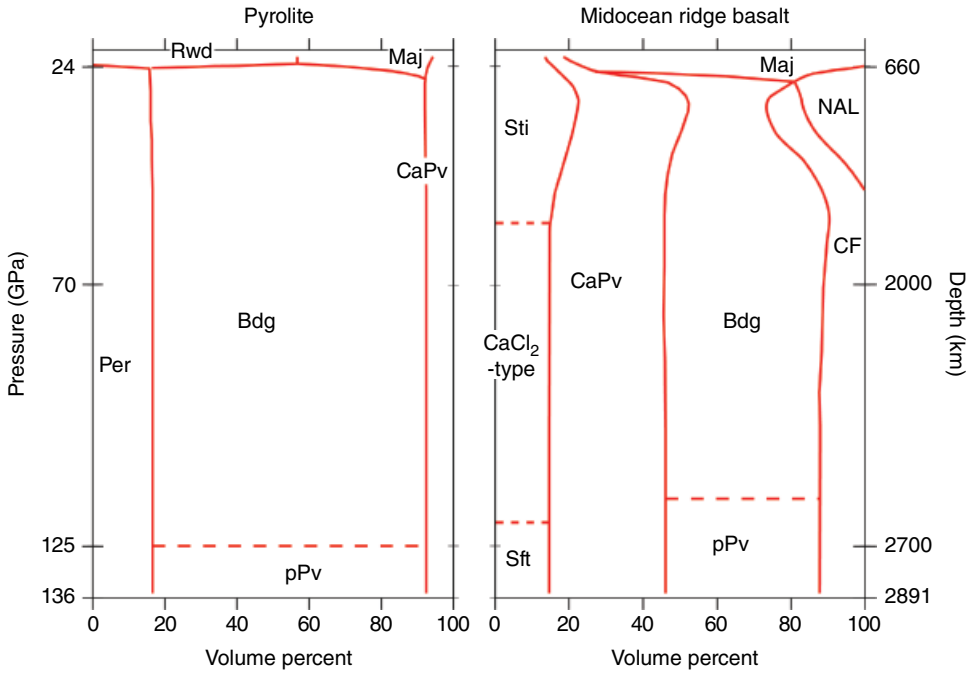

Figure 6.1 Expected volume fractions of lower mantle minerals for the pyrolite and midocean ridge basalt compositional models. Dashed lines indicate isochemical phase transitions, the exact locations of which depend on the mantle temperature profile. Mineral abbreviations are: Bdg, bridgmanite; Per, (ferro)periclase; Maj, majorite; Rwd, ringwoodite; Sti, stishovite; Sft, seifertite. Other abbreviations: CaPv, calcium-silicate perovskite; CF, calcium ferrite-type phase; NAL, new aluminous phase; pPv, post-perovskite. Adapted from *Hirose et al.* [2005]; *Irifune et al.* [2010], and *Ricolleau et al.* [2010].

on experimental and petrological studies of the peridotites and basalts of the uppermost mantle and assumes that the lower mantle composition is broadly similar to that of the upper mantle [*Ringwood*, 1975]. In pyrolite, bridgmanite, periclase, and perovskite-structured $CaSiO_3$ are the major minerals found in experiments across most of the lower mantle pressure range [*Kesson et al.*, 1998; *Irifune et al.*, 2010; *Irifune and Tsuchiya*, 2015]. There is geophysical evidence that subducting oceanic lithosphere penetrates the 660 km discontinuity, thereby transporting oceanic crust in the deep mantle, perhaps reaching as far as the core-mantle boundary. Subducted basaltic crust is expected to produce a different mineralogy, with increased Ca-perovskite together with free silica and aluminum-bearing phases (Figure 6.1) [*Irifune and Ringwood*, 1993; *Ono et al.*, 2001; *Hirose et al.*, 2005; *Ricolleau et al.*, 2010].

6.2. BRIDGMANITE, $(Mg,Fe)SiO_3$

The major mineral phase in the lower mantle and the most abundant mineral in Earth is $(Mg,Fe)SiO_3$ in the perovskite structure, now known as bridgmanite [*Tschauner et al.*, 2014]. The perovskite structure has the general formula ABX_3 and is adopted by materials encompassing a wide range of compositions. The A site is occupied by a large-radius cation, the B site contains a smaller cation, and the X site is an anion, typically oxygen or fluorine. The structure can be described as a framework of BX_6 octahedra forming a corner-sharing network with A cations nestled in the framework cavities (Figure 6.2). In an ideal cubic perovskite (space group $Pm\bar{3}m$), the large A cations are in 12-fold dodecahedral coordination with the anion, but when a smaller cation (such as Mg^{2+}) occupies the A site, the octahedral framework collapses around the cation such that the coordination decreases to eightfold [*Horiuchi et al.*, 1987].

Considerable structural diversity in perovskites can be introduced by rotation and tilting of octahedra, as well as through the effects of cation offsets, cation ordering, and nonstoichiometry [*Wang and Angel*, 2011]. Octahedral tilting alone can lead to a number of variants with tetragonal, orthorhombic, or monoclinic symmetry. Perovskite-structured $MgSiO_3$, first synthesized by *Liu* [1975], is orthorhombic with the $GdFeO_3$-type structure (space group *Pbnm* or *Pnma*, Table 6.1) and is isostructural with the mineral perovskite, $CaTiO_3$. The space group *Pnma* is equivalent to *Pbnm*, with the following

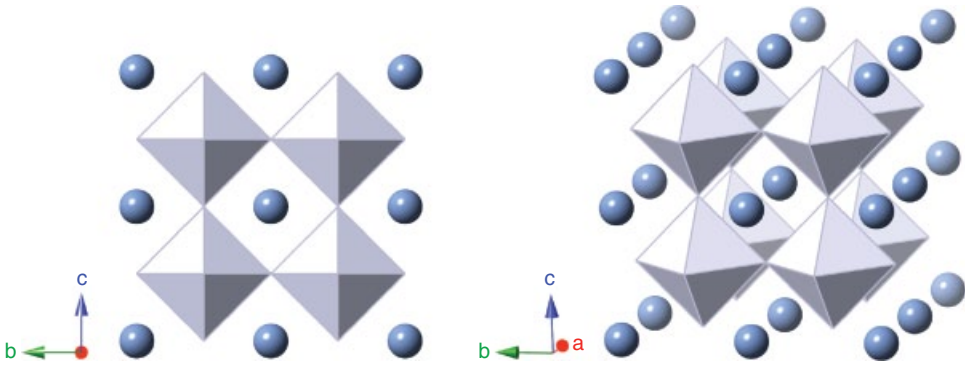

Figure 6.2 Cubic perovskite structure (space group $Pm\bar{3}m$, Table 6.1) of $CaSiO_3$ at conditions of the lower mantle. Spheres are Ca^{2+} cations each surrounded by 12 O^{2-} anions. Si^{4+} cations are centered among 6 O^{2-} anions in an octahedral arrangement, corner shared with adjacent octahedra.

Table 6.1 Crystallographic parameters for major lower mantle structures.

	x/a	*y/b*	*z/c*
Bridgmanite, (Mg,Fe)SiO_3[a] SG = *Pnma*[b], *a* = 5.02(3) Å, *b* = 6.90(3) Å, *c* = 4.81(2) Å			
Mg/Fe (4*c*)	0.557(2)	1/4	0.513(3)
Si/Fe (4*b*)	0	0	½
O (4*c*)	0.931(1)	1/4	0.381(3)
O (8*d*)	0.176(3)	0.575(1)	0.160(2)
Ferropericlase, (Mg,Fe)O[c] SG = $Fm\bar{3}m$, *a* = 4.211(1) Å			
Mg/Fe (4*a*)	0	0	0
O (4*b*)	½	½	½
Ca-perovskite, $CaSiO_3$[d] SG = $Pm\bar{3}m$, *a* = 3.546 Å			
Ca (1*b*)	½	½	½
Si (1*a*)	0	0	0
O (3*d*)	½	0	0
$CaIrO_3$-type post-perovskite, (Mg,Fe)SiO_3[e] SG = *Cmcm*, *a* = 2.466(1) Å, *b* = 8.130(6) Å, *c* = 6.108(10) Å			
Mg (4*c*)	0	0.256(2)	1/4
Si (4*a*)	0	0	0
O1 (4*c*)	0	0.929(5)	1/4
O2 (8*f*)	0	0.639(4)	0.437(5)

[a] $(Mg_{0.75}Fe_{0.20}Na_{0.03}Ca_{0.02}Mn_{0.01})Si_{1.00}O_3$, ambient pressure [*Tschauner et al.*, 2014].
[b] The space group *Pnma* is equivalent to *Pbnm*.
[c] MgO, ambient pressure [*Hazen*, 1976].
[d] Theoretical, ambient pressure [*Caracas and Wentzcovitch*, 2006].
[e] $Mg_{0.93}Fe_{0.07}SiO_3$, 121 GPa [*Zhang et al.*, 2013].

conversion: $(a,b,c)_{Pnma} \rightarrow (b,c,a)_{Pbnm}$. Deviation from the ideal cubic arrangement is achieved through both rotation (11.2° about the *c* axis at room pressure in *Pbnm*) and tilting (16.7° with respect to the *c* axis) of SiO_6 octahedra and offset in position of the central Mg atom [*Horiuchi et al.*, 1987] (Figure 6.3). These structural distortion increase with increasing pressure [*Fiquet et al.*, 2000].

While bridgmanite can be quenched to ambient conditions in the laboratory, direct evidence for the natural existence of this phase proved elusive for many years. Inclusions in rare diamonds of deep origin were interpreted as breakdown products of bridgmanite [*Harte and Harris*, 1994; *Stachel et al.*, 2000]. Recently, the first natural occurrence of this phase was definitively identified in a chondritic meteorite [*Tschauner et al.*, 2014], allowing assignment of the name bridgmanite. The natural sample had the composition $(Mg_{0.75}Fe_{0.20}Na_{0.03}Ca_{0.02}Mn_{0.01})Si_{1.00}O_3$ and was found in association with akimotoite, a magnesium silicate with the ilmenite-type structure. The formation conditions for the bridgmanite sample were estimated to be 23–25 GPa and 2200–2400 K.

A wide range of cations can occupy the A and B sites in perovskites. Bridgmanite itself can accommodate increasing amounts of Fe and Al under compression [*Mao et al.*, 1997; *Ito et al.*, 1998]. Substitution of Fe^{2+} for Mg^{2+} in the A site of perovskite expands the structure and decreases the degree of distortion [*Kudoh et al.*, 1990]. Substitution of Fe^{3+} similarly expands the structure but can increase the degree of distortion as a result of a coupled substitution mechanism involving both the A and B sites [*Catalli et al.*, 2010]. Incorporation of aluminum into bridgmanite can occur by either a Tschermak-like coupled stoichiometric substitution:

$$Mg^{2+} + Si^{4+} = 2Al^{3+}, \tag{6.1}$$

or through nonstoichiometric substitution involving an oxygen vacancy, $V_O^{\cdot\cdot}$:

$$2Si^{4+} = 2Al^{3+} + V_O^{\cdot\cdot}. \tag{6.2}$$

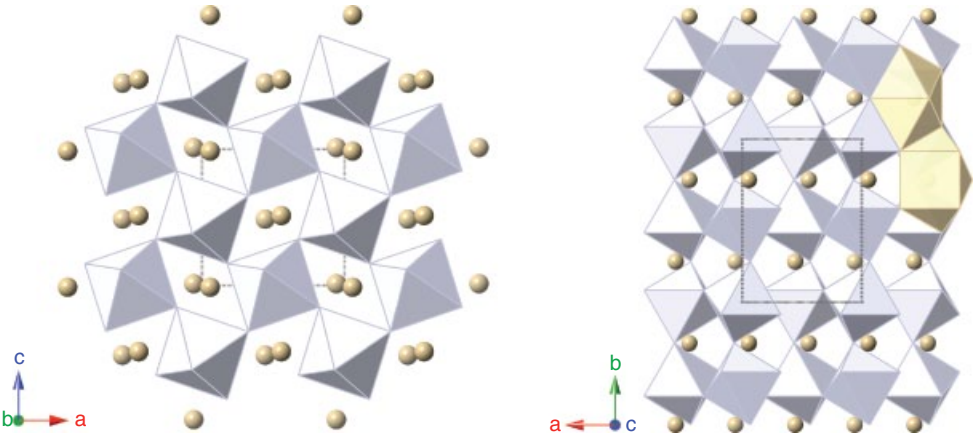

Figure 6.3 View along the *b* (left) and *c* axis (right) of bridgmanite (*Pnma*, Table 6.1). Gray dashed line shows the outline of the unit cell. Tilting of SiO_6 octahedra (blue) results in shortening of crystallographic axes and produces a displacement of Mg cations (yellow spheres and representative MgO_6 polyhedra) reducing the coordination from 12 to 8.

At pressures of the lower mantle, the stoichiometric substitution (6.1) is energetically favorable [*Brodholt*, 2000; *Yamamoto et al.*, 2003; *Akber-Knutson and Bukowinski*, 2004], yet there is experimental evidence for the operation of both substitution mechanisms in laboratory-synthesized samples. Nuclear magnetic resonance results are consistent with two distinct Al sites, indicating coupled substitution [*Stebbins et al.*, 2001], while the enhanced compressibility observed in some equation-of-state studies is more consistent with vacancy substitution [*Andrault et al.*, 2007]. Al^{3+} substitution increases both the unit cell volume and its degree of distortion, possibly as a result of less efficient packing due to substitution in both the A and B sites, leading to an $(Mg,Al)(Si,Al)O_3$ composition [*Weng et al.*, 1982]. This is consistent with the results of a structure refinement study comparing perovskites synthesized with both substitution mechanisms: "stoichiometric" Al-containing $MgSiO_3$ perovskites are more distorted than their "non-stoichiometric" counterparts [*Kojitani et al.*, 2007a]. The perovskite structure can accommodate up to 25 mol.% aluminum, as both pyrope and almandine garnets have been shown to adopt the perovskite structure at sufficiently high pressures [*Ito et al.*, 1998; *Kesson et al.*, 1995; *Dorfman et al.*, 2012].

Coupled substitution of Fe^{3+} and Al^{3+} allows both cations to be preferentially incorporated into the bridgmanite phase, stabilizing Fe^{3+} even under the more reducing conditions of the lower mantle [*Frost and McCammon*, 2008]. This capacity to host Fe with such high oxidation state allows for a lower mantle enriched in Fe^{3+} and one that potentially contains metallic iron as part of the equilibrium assemblage. A disproportionation of Fe^{2+} to Fe^{3+} + Fe^0 has been proposed on the basis of closed-system experiments observing the latter [*Frost et al.*, 2004; *Auzende et al.*, 2008].

The nature of the spin-pairing crossover of Fe in bridgmanite has been the subject of considerable debate from both experimental and theoretical viewpoints [e.g., *Lin et al.*, 2013]. The behavior of Fe in Mg-perovskite is inherently complex due to iron's potential to adopt multiple structural sites (A or B), valence states (2+, 3+), and electronic configurations (high, low, and potentially intermediate spin). It appears that Fe^{2+} in bridgmanite does not undergo a spin crossover at lower mantle pressures but does exhibit a large change in quadrupole splitting as a function of pressure, consistent with a marked increase in lattice distortion of the A site [*Jackson et al.*, 2005; *Hsu et al.*, 2010]. For ferric iron-containing perovskite, the evidence indicates that Fe^{3+} in the smaller B undergoes a transitions to a low-spin state by 60 GPa, whereas Fe^{3+} in the larger A site remains in the high-spin configuration [*Catalli et al.*, 2010].

Over the pressure range of the lower mantle, the maximum solubility of Fe^{2+} in bridgmanite increases. In Al-free samples, a maximum solubility of Fe/(Mg+Fe) ranges from 0.16 at 25 GPa, 1500°C [*Tange et al.*, 2009] to at least 0.74 at 80 GPa [*Dorfman et al.*, 2013]. Recent laser-heated diamond anvil experiments reported unexpectedly that at pressures of 95 GPa (~2100 km depth) and temperatures above 2200 K, Fe-bearing bridgmanite disproportionates into an iron-poor bridgmanite phase and a previously unknown iron-rich silicate [*Zhang et al.*, 2014]. If confirmed, this finding could have major relevance for understanding the deep mantle.

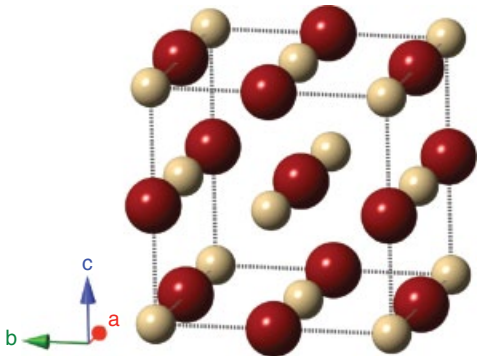

Figure 6.4 Rocksalt structure of ferropericlase (Mg,Fe)O ($Fm\bar{3}m$, Table 6.1). Interpenetrating Mg/Fe (yellow spheres) and O (red spheres) lattices result in octahedral coordination of both cations and anions.

6.3. FERROPERICLASE, (Mg,Fe)O

Ferropericlase, (Mg,Fe)O, is the second most abundant phase in pyrolite compositions in the lower mantle (Figure 6.1). This phase adopts the simple rocksalt (B1) structure (space group $Fm\bar{3}m$) consisting of interpenetrating face-centered-cubic lattices producing alternating Mg^{2+}/Fe^{2+} cations and O^{2-} anions (Figure 6.4). The structure can also be described as an edge-share array of $(Mg,Fe)O_6$ octahedra in which all edges are shared with neighboring octahedra. High pressure-temperature (*P-T*) partitioning studies between ferropericlase and bridgmanite indicate that iron partitions preferentially into ferropericlase such that this mineral is expected to have compositions around Mg/(Mg+Fe) = 0.8 under mantle conditions [*Auzende et al.*, 2008; *Sakai et al.*, 2009; *Tange et al.*, 2009] and that iron in (Mg,Fe)O is predominately in the ferrous state [*McCammon et al.*, 1998]. Ferropericlase also undergoes a spin-pairing transition at lower mantle conditions, and the effects of this transition on density, elastic properties, partitioning behavior, and transport properties have been the subjects of intensive recent study [*Badro et al.*, 2003; *Sturhahn et al.*, 2005; *Bower et al.*, 2009; *Lin et al.*, 2013; *Badro*, 2014].

While the Mg end-member periclase is expected to be stable throughout the lower mantle pressure range [*Duffy et al.*, 1995], the Fe end-member, wüstite, displays more complex behavior. At room temperature, FeO first undergoes a distortion to a rhombohedral structure (space group $R\bar{3}m$) [*Mao et al.*, 1996; *Shu et al.*, 1998] followed by transition to the hexagonal B8 phase (space group $P6_3mc$) [*Fei and Mao*, 1994; *Murakami et al.*, 2004a] at ~120 GPa. At the high *P-T* conditions expected along a mantle geotherm, FeO is expected remain in the B1 structure, yet experiments suggest it will undergo an insulator-metal transition near 70 GPa and 1900 K [*Fischer et al.*, 2011]. Such a phase transition in the end-member composition suggests that the Mg^{2+}-Fe^{2+} solid solution, complete at low pressures, would no longer be continuous above the transition pressure. At present, experimental confirmation of this is inconclusive as evidence for and against dissociation has been reported [*Dubrovinsky et al.*, 2000; *Lin et al.*, 2003; *Kondo et al.*, 2004; *Ohta et al.*, 2014].

FeO may exist at the core-mantle boundary as a result of reaction with the liquid outer core metallic alloy [*Manga and Jeanloz*, 1996; *Buffett and Seagle*, 2010]. Such a metallic component in the lowermost mantle could have implications for phase relations, electrical conductivity, and coupling between the core and mantle [*Seagle et al.*, 2008]. Iron-rich ferropericlase may also provide an explanation for ultra-low seismic velocity zones observed near the CMB [*Wicks et al.*, 2010].

6.4. $CaSiO_3$ PEROVSKITE

Calcium silicate perovskite ($CaSiO_3$, Ca-Pv) is considered to be the third most abundant phase in the lower mantle, comprising ~10% by volume of a pyrolite composition and up to ~25 vol % of the abundance in basaltic regions [*Irifune et al.*, 2010; *Ricolleau et al.*, 2010] (Figure 6.1). This phase was first synthesized at high pressure and temperature by *Liu and Ringwood* [1975]. It is unquenchable and transforms to glass at ambient conditions [*Tamai and Yagi*, 1989]. The crystal structure at 300 K was originally reported to be cubic perovskite $\left(Pm\bar{3}m\right)$ [*Liu and Ringwood*, 1975; *Mao et al.*, 1989; *Wang and Weidner*, 1994] (Figure 6.2). Later theoretical calculations indicated that the cubic form was unstable at low temperatures as a result of slight rotations of the SiO_6 octahedra [*Stixrude et al.*, 1996]. A structural distortion was subsequently confirmed by experiment [*Shim et al.*, 2002]. The nature of this low-temperature noncubic distortion has been the subject of extensive theoretical investigations with both tetragonal [*Stixrude et al.*, 1996; *Caracas et al.*, 2005] and orthorhombic [*Jung and Oganov*, 2005; *Adams and Oganov*, 2006; *Li et al.*, 2006a] forms being proposed.

At elevated temperatures, Ca-Pv transforms into the cubic structure. While one study has found that the noncubic form remains stable up to 18 GPa and 1600 K [*Uchida et al.*, 2009], most studies find that Ca-Pv becomes cubic at relatively low temperatures (<600 K) [*Kurashina et al.*, 2004; *Ono et al.*, 2004; *Komabayashi et al.*, 2007; *Noguchi et al.*, 2012; *Sun et al.*, 2014]. Thus, the cubic form is expected to be the relevant one for Earth's mantle. Theoretical calculations predict a low shear modulus that could potentially be relevant to low shear velocity anomalies in the deep mantle [*Kawai and Tsuchiya*, 2015].

Experiments exploring the mutual solubility of the two perovskites (Mg into Ca-Pv and Ca into bridgmanite) find substitution to be very limited in the uppermost lower mantle, but that up to 10% Mg can be substituted

into Ca-Pv by 55 GPa [*Armstrong et al.*, 2012]. This effect is enhanced with pressure, temperature, and the substitution of Ti^{4+} for Si^{4+}, with Mg-Ca forming a complete solution at 97 GPa for modest amounts of Ti substitution (Ti/(Ti+Si) = 0.05).

6.5. $CaIrO_3$-TYPE POST-PEROVSKITE PHASE

While $MgSiO_3$ bridgmanite is stable throughout most of the lower mantle, at pressures near 125 GPa and ~2500 K (corresponding to the D″ region near the core-mantle boundary), it transforms to a high-pressure polymorph known as "post-perovskite" [*Murakami et al.*, 2004b; *Oganov and Ono*, 2004]. This phase adopts the orthorhombic $CaIrO_3$-type structure (space group *Cmcm*). In post-perovskite, Si^{4+} and Mg^{2+} have the same coordination environment as in perovskite, but there are profound differences in their structural arrangement. In contrast to the corner-sharing network in perovskite, the SiO_6 octahedra in post-perovskite share edges along the *a* axis and corners along *c*. The structure is thus sheet-like with layers of SiO_6 octahedra alternating with MgO_8 layers along the *b* axis (Figure 6.5). The Mg sites in post-perovskite are smaller and less distorted than those in Pv, resulting in a volume reduction of ~1–1.5% across the transition.

Experimental studies of the structure of the post-perovskite phase have mainly been carried out using powder X-ray diffraction techniques [*Murakami et al.*, 2004b; *Shim et al.*, 2008; *Hirose et al.*, 2015]. First-principles studies of the structure and its pressure evolution are generally consistent with experiment results [*Oganov and Ono*, 2004; *Lin et al.*, 2014]. Some evidence for slight structural modifications of the post-perovskite structure have been reported on the basis of polycrystalline X-ray studies in aluminum-rich [*Tschauner et al.*, 2008] and iron-rich compositions [*Yamanaka et al.*, 2012], but these have not yet been confirmed. Recently, a single-crystal structure refinement of $(Mg,Fe)SiO_3$ post-perovskite was carried out to very high pressures of 120 GPa by isolating individual crystals for study from a coarse multigrain aggregate that was synthesized in the diamond anvil cell [*Zhang et al.*, 2013].

The anisotropic nature of the post-perovskite structure likely has a number of geophysical implications. The compressibility in the *b* direction is substantially higher than in *a* or *c* due to the presence of the relatively soft MgO_8 layer [*Iitaka et al.*, 2004]. Theoretical calculations indicate that post-perovskite also has larger elastic shear wave anisotropy than perovskite. The mode of deformation is being studied extensively in both silicate and analog compositions to attempt to explain the observed seismic anisotropy in the deep mantle in terms of the deformation behavior and elastic anisotropy of post-perovskite, with no definitive answer as of yet [*Oganov et al.*, 2005; *Yamazaki et al.*, 2006; *Merkel et al.*, 2007; *Miyagi et al.*, 2010; *Dobson et al.*, 2013]. Theoretical studies have also shown that, in contrast to bridgmanite, diffusion in post-perovskite is highly anisotropic [*Ammann et al.*, 2010] and that thermal conductivity of post-perovskite is both more anisotropic and larger than in perovskite [*Ammann et al.*, 2014]. These factors may be important for understanding the viscosity and heat flow at the base of the mantle.

6.6. SiO_2 POLYMORPHS

Mid-ocean ridge basalt compositions are rich in SiO_2 relative to pyrolite, and the resulting mineral assemblage is expected to contain ~10–20% free silica at lower mantle conditions (Figure 6.1) [*Irifune and Ringwood*, 1993;

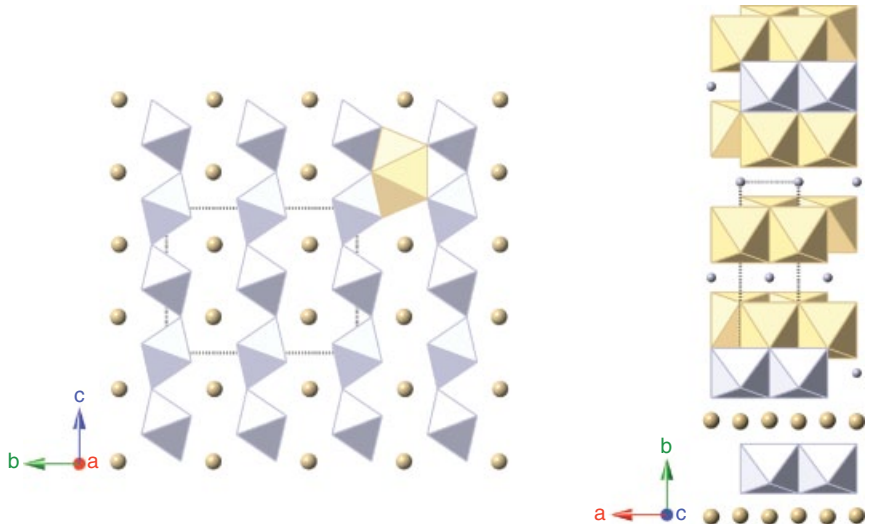

Figure 6.5 Crystal structure of $CaIrO_3$-type post-perovskite (space group *Cmcm*, Table 6.1) viewed along *a* (left) and *c* axis (right). Gray dashed line shows the outline of unit cell. The structure consists of "sheets" of edge-shared SiO_6 octahedra (gray) that are intercalated by Mg ions (yellow spheres and polyhedra).

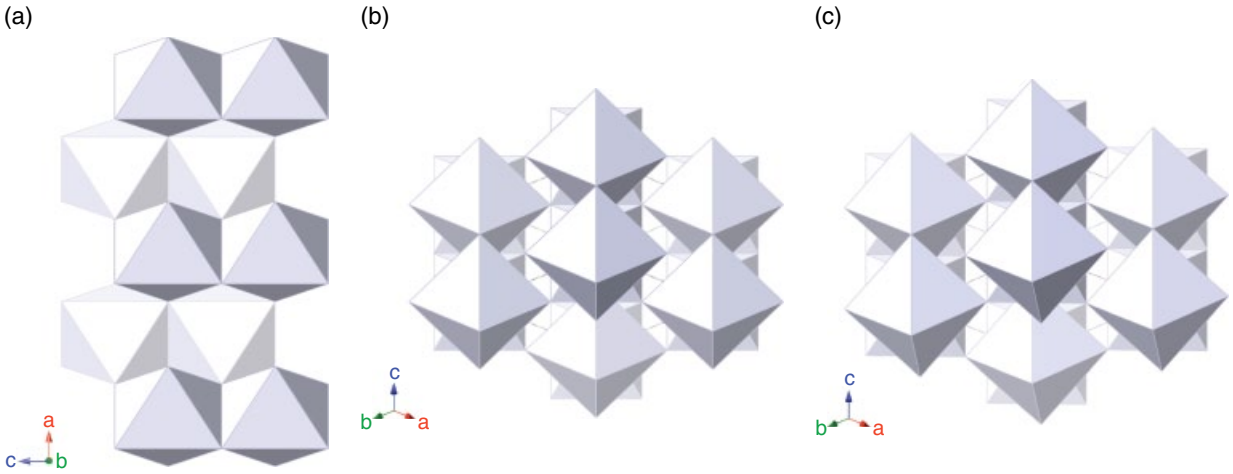

Figure 6.6 (a) Structure of rutile-type stishovite (space group $P4_2/mnm$, Table 6.2) along the *b* axis. SiO_6 octahedra (blue) are organized into edge-sharing chains that extend along the *c* direction and connect to neighboring chains by corner sharing. The figure is depth shaded to illustrate offset in the octahedra. Slight rotation difference between the octahedra of (b) stishovite and (c) $CaCl_2$-type (space group *Pnnm*, Table 6.2) structures can be seen when viewed 45° from the a, b, and c axes. Octahedral tilting reduces the symmetry from tetragonal to orthorhombic and the amount of tilt increases with pressure [*Andrault et al.*, 1998].

Table 6.2 Crystallographic parameters of SiO_2 polymorphs in the lower mantle.

	x/a	*y/b*	*z/c*
Stishovite, SiO_2[a] SG = $P4_2/mnm$, a = 4.1812(1) Å, c = 2.6662(3) Å			
Si (2*a*)	0	0	0
O (4*f*)	0.3063(1)	0.3063(1)	0
$CaCl_2$-type SiO_2[b] SG = *Pnnm*, a = 3.7201(9) Å, b = 3.9422(10) Å, c = 2.4913(3) Å			
Si (2*a*)	0	0	0
O (4*g*)	0.276	0.313	0
Seifertite, SiO_2[c] SG = *Pbcn*, a = 4.097(1) Å, b = 5.0462(9) Å, c = 4.4946(8) Å			
Si (4*c*)	0	0.1522(9)	¼
O (8*d*)	0.7336(16)	0.6245(12)	0.9186(29)

[a] Ambient pressure [*Yamanaka et al.*, 2002].
[b] 120 GPa [*Andrault et al.*, 1998].
[c] Ambient pressure [*Dera et al.*, 2002].

Ricolleau et al., 2010]. Stishovite, which becomes the stable form of SiO_2 at pressures above ~7 GPa, crystallizes in the tetragonal rutile-type structure (space group $P4_2/mnm$) [*Stishov and Belov*, 1962]. This structure consists of slightly distorted SiO_6 octahedra that share edges to form chains running parallel to the *c* axis (Figure 6.6a). Each octahedron is corner linked to four neighboring chains. The structure can also be described as a distorted hexagonal close-packed array of O^{2-} anions with half of the octahedral sites occupied. A number of structural studies of stishovite have been reported at both ambient [*Sinclair and Ringwood*, 1978; *Hill et al.*, 1983] and high pressures [*Sugiyama et al.*, 1987; *Ross et al.*, 1990]. Stishovite has been observed naturally as an inclusion phase in diamonds of deep origin [*Joswig et al.*, 1999] and as a product of transient high pressure-temperature meteorite impact events [*Chao et al.*, 1962].

At ~50 GPa, stishovite undergoes a displacive phase transition to the orthorhombic $CaCl_2$-type structure (orthorhombic, space group *Pnnm*) [*Cohen*, 1987; *Tsuchida and Yagi*, 1989; *Kingma et al.*, 1995]. This structure differs from stishovite only by a small rotation of the octahedral chains (Figure 6.6c). The transition is driven by the softening of a zone-center optic mode that couples with acoustic modes to produce a marked softening of the shear elastic constants [*Cohen*, 1992; *Karki et al.*, 1997a; *Jiang et al.*, 2009; *Asahara et al.*, 2013]. As a result, even a small fraction of free silica may produce a detectable seismic signal in the mid-lower mantle [*Karki et al.*, 1997a]. Several studies have attempted to associate this transition with seismic reflectors observed at greater than 800 km depth [*Kawakatsu and Niu*, 1994; *Vinnik et al.*, 2001, 2010]. The *P-T* phase boundary for the post-stishovite transition has been examined a number of times [*Kingma et al.*, 1995; *Ono et al.*, 2002; *Tsuchiya et al.*, 2004; *Nomura et al.*, 2010]. *Nomura et al.* [2010] reported a positive Clapeyron slope for the transition and predicted a transition pressure of ~70 GPa along a typical mantle geotherm and 56 GPa for conditions appropriate to a subducting slab. These correspond

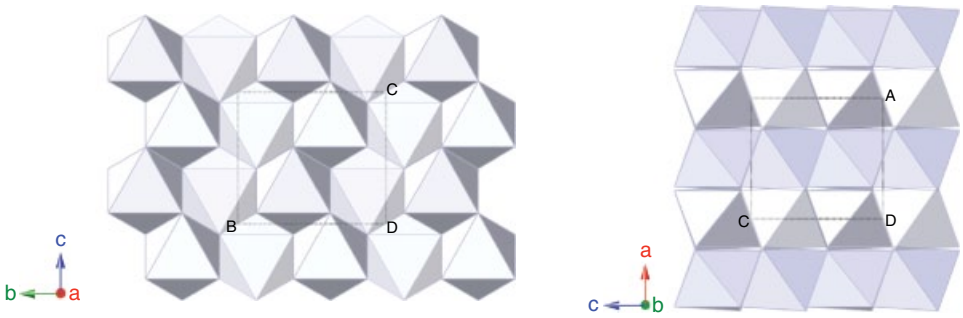

Figure 6.7 Structure of α-PbO_2-type SiO_2, seifertite (space group, *Pbcn*, Table 6.2), viewed along the *a* (left) and *b* axis (right). The octahedra are depth shaded to aid in distinguishing top layers of SiO_6 octahedra, dark blue, from underlying layers, lighter blue. Unlike the stishovite and the $CaCl_2$-type structures (Figure 6.6), the SiO_6 octahedra are organized into kinked chains that allow both for more efficient packing and less-distorted octahedra.

to depths of about 1400–1700 km in the mantle. Incorporation of aluminum and water into SiO_2, however, has been shown to markedly reduce the post-stishovite transition pressure [*Lakshtanov et al.*, 2007; *Bolfan-Casanova et al.*, 2009].

At yet higher pressures, SiO_2 undergoes a further transformation to seifertite, which has the scrutinyite (α-PbO_2-type, space group *Pbcn*) structure [*Murakami et al.*, 2003; *Dubrovinsky et al.*, 2001; *Belonoshko et al.*, 1996; *Grocholski et al.*, 2013]. In this phase, distorted SiO_6 octahedra are arranged into kinked chains extending along the *c* axis, resulting in a small density increase compared with stishovite and the $CaCl_2$-type phase (Figure 6.7). The reported transition pressure is close to that of Earth's CMB, but it is not yet clear if this phase would definitely be expected to exist in the D″ region just above the CMB [*Murakami et al.*, 2003; *Shieh et al.*, 2005; *Grocholski et al.*, 2013]. The presence of aluminum appears to have a modest effect in reducing the transition pressure, which may be enough to stabilize the phase in Earth's deep lower mantle [*Andrault et al.*, 2014].

Seifertite has also been found in a number of meteorites where it appears to have experienced shock pressures well below those of the expected stability field [*Sharp et al.*, 1999; *Dera et al.*, 2002; *Goresy et al.*, 2008]. Theoretical studies have shown that there exists a large family of closely related and energetically competitive phases of SiO_2 with closed-packed oxygen anions and different arrangements of Si in the octahedral sites [*Teter et al.*, 1998]. As a result, the metastable formation of silica structures may occur under various conditions, and this may explain the observation of seifertite in meteorites [*Kubo et al.*, 2015]. In laboratory studies, the observed phase may depend on starting material, stress conditions, or *P-T* path. There have been reports of the occurrence of seifertite or a related structure at much lower pressures (~80 GPa) in some high-temperature experiments [*Dubrovinsky et al.*, 1997, 2001] or upon compression of cristobalite starting material at room temperature to ~50 GPa [*Dubrovinsky et al.*, 2001; *Shieh et al.*, 2005].

6.7. ALUMINOUS PHASES

Two aluminum-rich phases expected in basalt lithologies at high pressures are the "new aluminous phase" (NAL) and a phase with the Ca-ferrite structure (called the "CF phase") (Figure 6.1). Together, these two phases may account for 10–25 vol.% of subducting basaltic crust in the lower mantle [*Ono et al.*, 2001; *Ricolleau et al.*, 2010; *Irifune and Ringwood*, 1993]. The Ca-ferrite structure is a common high-pressure structure type adopted by several compositions including $MgAl_2O_4$ [*Irifune et al.*, 1991], $CaAl_2O_4$ [*Reid and Ringwood*, 1969], and $NaAlSiO_4$ [*Liu*, 1977]. It is one of a series of similar structures ($CaFe_2O_4$, $CaTi_2O_4$, $CaMn_2O_4$) that are common high-pressure polymorphs of spinel-structured phases [*Yamanaka et al.*, 2008]. Single-crystal diffraction experiments have recently shown that forsterite, Mg_2SiO_4, metastably adopts a related structure upon room temperature compression above 58 GPa [*Finkelstein et al.*, 2014].

The general formula for the Ca-ferrite structure is XY_2O_4 where the eight-fold coordinated X site can be occupied by the mono- and divalent cations K^+, Na^+, Ca^{2+}, and Mg^{2+}, and the six-coordinated Y sites are occupied by Al^{3+} and Si^{4+}. The structure is orthorhombic (space group *Pbnm*) (Figure 6.8), and consists of edge-sharing double chains of octahedra that form tunnels parallel to the *c* axis with the X cations occupying spaces between the double chains.

The NAL phase is hexagonal (space group $P6_3/m$) and has the general formula $AX_2Y_6O_{12}$ where A is a nine-fold coordinated channel site typically occupied by large mono or divalent cations such as Na^+ or K^+ or Ca^{2+} [*Gasparik et al.*, 2000; *Miura et al.*, 2000; *Miyajima*

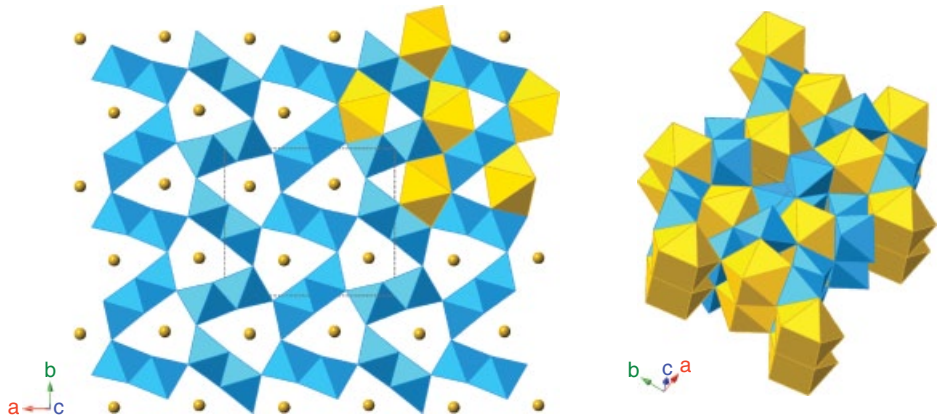

Figure 6.8 Calcium ferrite-type structure (space group *Pbnm*, Table 6.3) viewed along (left) and oblique (right) to the *c* axis. AlO_6 octahedra (light blue) edge share to form double chains extending along the *c* axis. Eight-fold coordinated cations (yellow spheres and polyhedra) are located in channels made up of four double chains–two edge-on and two face-on. This model is based on structural parameters for the $MgAl_2O_4$ end-member [*Kojitani et al.*, 2007b], whereas the Ca-ferrite-type phase in basaltic compositions of the mantle can exist within the $NaAlSiO_4$-$MgAl_2O_4$ system.

et al., 2001] (Figure, 6.9). The X site is six-coordinated but trigonal prismatic rather than octahedral and is typically occupied by Mg^{2+} or Fe^{2+}. The octahedrally coordinated Y site is occupied by Al^{3+} or Si^{4+}. Like the Ca-ferrite structure, the distorted Y octahedra form edge-sharing double chains extending along the *c* axis that are corner linked to form tunnels. Within the tunnels lie the larger A sites while the smaller X sites are surrounded by three double chains. With multiple sites that can each accept more than one cation, the NAL structure can accommodate a wide range of compositional variation.

The large cation sites in the NAL and CF structure allow them to be potential hosts for the alkali elements in subducted crust. Of the two structures, NAL more readily accommodates large ions due to its nine-fold site [*Miyajima et al.*, 2001]. Theoretical studies indicate that pressure tends to favor the stability of the CF phase with respect to NAL, but that NAL is stabilized by Mg^{2+} or alkali element enrichment [*Kawai and Tsuchiya*, 2012; *Mookherjee et al.*, 2012]. As a result, the relative abundance of these phases in the lower mantle will depend on composition. K-free NAL was shown to become unstable above 27 GPa and 1850 K [*Imada et al.*, 2011]. Previous studies of basaltic compositions showed that the NAL phase was only stable to ~40 GPa [*Ricolleau et al.*, 2010]. However, it has been shown that K-rich NAL [*Kojitani et al.*, 2011] is stable throughout the lower mantle pressure range [*Kato et al.*, 2013] and could exist in deeply subducted sediments or continental crust [*Kawai et al.*, 2009; *Komabayashi et al.*, 2009]. K-rich NAL may then be a host for K in the deep mantle and could contribute to radiogenic heating in the deep Earth [*Kato et al.*, 2013]. Recently, inclusion compositions in diamonds inferred to originate from the lower mantle have provided evidence for the CF and NAL phases in natural samples for the first time [*Walter et al.*, 2011]. Structural differences between these two phases lead to distinct physical properties—density functional theory calculations show that the NAL phase has low seismic velocities compared to the CF phase, and NAL could contribute to low-velocity provinces in the deep mantle [*Mookherjee et al.*, 2012].

6.8. POSSIBLE HYDROUS PHASES

There is considerable interest in the potential role of hydrogen in deep-mantle crystal structures, as the presence of hydrogen, even in small quantities, can strongly affect physical and chemical properties such as melting, viscosity, phase transitions, and seismic velocities. In the upper mantle, a variety of crystal structures can accommodate hydrogen, especially under lower temperature conditions of subducting slabs. Nominally anhydrous minerals such as wadsleyite and ringwoodite are potential hosts for water in the transition zone [*Smyth*, 1987; *Kohlstedt et al.*, 1996; *Pearson et al.*, 2014]. The role of hydrous phases in the lower mantle is only beginning to be explored but has been a growing focus of study in recent years.

6.8.1. Phase D

Among the hydrous magnesium silicates that are potential hosts for water in the upper mantle and transition zone [*Prewitt and Parise*, 2000], phase D has the highest pressure stability (to ~44 GPa and 1400°C, corresponding to depths of ~1250 km) [*Shieh et al.*, 1998]. This phase

Table 6.3 Crystallographic parameters of aluminous and hydrous phases in the lower mantle.

	x/a	*y/b*	*z/c*
Calcium ferrite-type $MgAl_2O_4$[a] SG = *Pbnm*, *a* = 9.9498(6) Å, *b* = 8.6468(6) Å, *c* = 2.7901(2) Å			
Mg (4*c*)	0.3503(4)	0.7576(6)	1/4
Al1 (4*c*)	0.3854(4)	0.4388(5)	1/4
Al2 (4*c*)	0.8964(3)	0.4159(4)	1/4
O1 (4*c*)	0.8344(7)	0.2005(8)	1/4
O2 (4*c*)	0.5279(7)	0.1201(6)	1/4
O3 (4*c*)	0.2150(7)	0.5357(8)	1/4
O4 (4*c*)	0.5709(6)	0.4089(7)	1/4
New aluminous phase, NAL[b] SG = $P6_3/m$, *a* = 8.7225(4) Å, *c* = 2.7664(2) Å			
M1 (6*h*)	0.98946(8)	0.34353(9)	1/4
M2 (2*d*)	2/3	1/3	1/4
M3 (2*a*)	0	0	1/4
O1 (6*h*)	0.1283(2)	0.5989(2)	1/4
O2 (6*h*)	0.3124(2)	0.2024(2)	1/4
Phase D, $MgSi_2H_2O_6$[c] SG = $P\bar{3}1m$, *a* = 4.7453(4) Å, *c* = 4.3450(5) Å			
Mg (1*a*)	0	0	0
Si (2*d*)	2/3	1/3	1/2
O (6*k*)	0.6327(2)	0	0.2716(2)
H[d] **(6*k*)**	0.536(13)	0	0.091(10)
Phase H, $MgSiH_2O_4$[e] SG = *Pnnm*, *a* = 4.733(2) Å, *b* = 4.325(1) Å, *c* = 2.842(1) Å			
Mg/Si (2*a*)	0	0	0
O (4*g*)	0.347(1)	0.230(1)	0
H[f] **(4*g*)**	0.475	0.042	0

[a] Ambient pressure [*Kojitani et al.*, 2007].
[b] $Na_{0.41}[Na_{0.125}Mg_{0.79}Al_{0.085}]_2[Al_{0.79}Si_{0.21}]_6O_{12}$, ambient pressure [*Pamato et al.*, 2014].
[c] $Mg_{1.11}Si_{1.89}H_{2.22}O_6$, ambient pressure [*Yang et al.*, 1997].
[d] Partial H occupancy of 0.37.
[e] Ambient pressure [*Bindi et al.*, 2014].
[f] Tentative H position, assumed occupancy of 0.50.

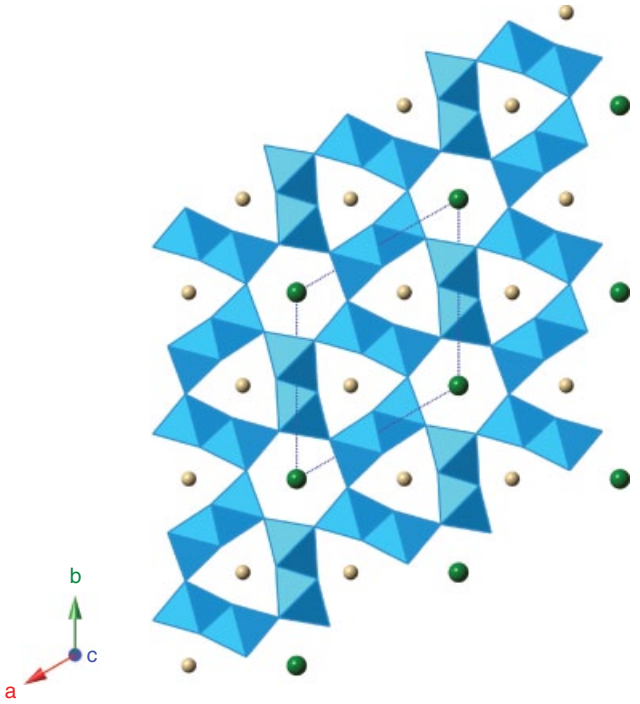

Figure 6.9 New aluminous phase, NAL (space group $P6_3/m$, Table 6.3) viewed along the c axis. Around each Mg^{2+} ion (small yellow spheres) are three double chains of AlO_6 octahedra (light blue) connected by corner-sharing oxygen ions. Large channels are formed by six SiO_6 octahedra in three double chains and are occupied typically by Na^+ or K^+ ions (large green spheres) at half occupancy.

can form upon breakdown of serpentine and could serve as a water carrier in cold lithosphere subducting into the lower mantle [*Liu*, 1986; *Frost and Fei*, 1998].

Phase D has the ideal formula $MgSi_2O_4(OH)_2$ but is typically nonstoichiometric. It crystallizes in the trigonal system (space group $P\bar{3}1m$) [*Kudoh et al.*, 1997; *Yang et al.*, 1997]. Oxygen anions form a hexagonal close-packed lattice with Si^{4+} and Mg^{2+} both occupying octahedral sites. The MgO_6 and SiO_6 octahedra are organized into alternating layers along the *c* direction. The SiO_6 octahedra form gibbsite-like layers in which each octahedron shares 3 edges, leaving one third of the octahedral sites vacant. MgO_6 octahedra lie above and below vacant sites in the SiO_6 layer and are corner linked to the Si octahedra, and so two thirds of the Mg octahedral sites are empty (Figure 6.10).

The hydrogen positions are located in the MgO_6 layers, with O-H bonds facing away from SiO_6 octahedra. Typically, approximately one third of the proton positions are occupied. Phase D exhibits considerable disorder and compositional variability as a function of synthesis conditions, with reported Mg/Si ratios variable between 0.55 and 0.71 and H_2O content variable between 10 and 18 wt.% [*Frost and Fei*, 1998]. Phase D can incorporate both aluminum and iron: the presence of Al in phase D has been shown to extend its stability field, although the presence of Fe counteracts this expansion [*Ghosh and Schmidt*, 2014]. Very recently an aluminum-rich variant of phase D ($Al_2SiO_4(OH)_2$) has been synthesized, and its stability field was found to extend to over 2000°C at 26 GPa [*Pamato et al.*, 2015]. Disordering of Al and Si cations renders the two previously distinct octahedral sites equivalent, increasing the symmetry and enhancing the stability of this phase.

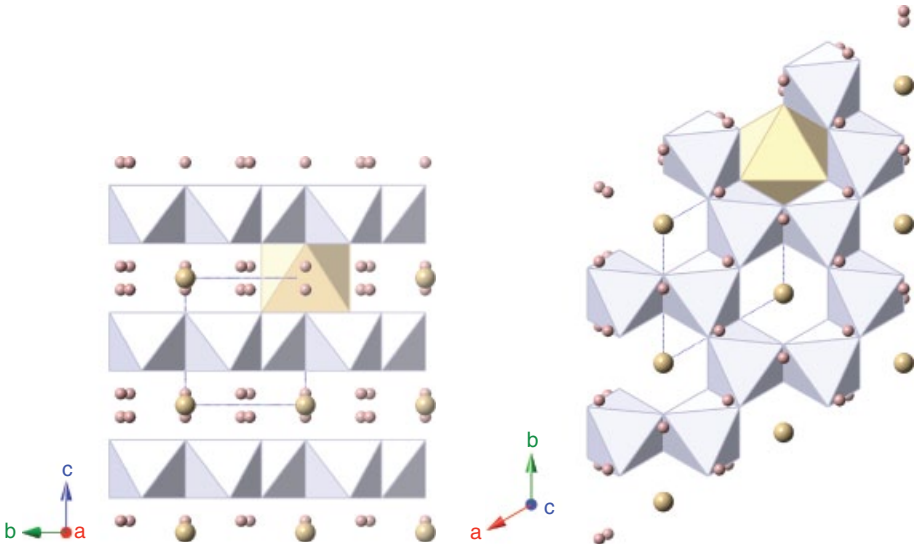

Figure 6.10 Dense hydrous magnesium silicate, phase D (space group $P\bar{3}1m$, Table 6.3), viewed along the *a* axis (left) and *c* axis (right). SiO_6 octahedra (blue) share edges with neighbors to form rings in layers perpendicular to the *c* axis. Mg cations (yellow spheres and representative MgO_6 polyhedron) partially occupy the spaces between the SiO_6 rings in alternating layers. Charge balance is achieved by hydrogen anions represented by small pink spheres.

Phase D exhibits anisotropic compression as a result of the layered nature of the structure, with strong SiO_6 layers alternating with weaker MgO_6 octahedra resulting in enhanced compressibility along the *c* axis [*Frost and Fei*, 1999]. Theoretical calculations of the elastic constants indicate that the anisotropy decreases with depth but significant anisotropy in seismic wave velocities is retained to the highest pressures [*Mainprice et al.*, 2007].

It has been suggested on theoretical grounds that hydrogen bonding in phase D will increasingly approach and finally reach a condition of symmetric bonding at ~40 GPa [*Tsuchiya et al.*, 2005]. A symmetric hydrogen bond is one in which the hydrogen atom is located at the midpoint between the two neighboring oxygen atoms, rather than the asymmetric O-H distances that characterize a conventional hydrogen bond. H bond symmetrization in phase D is predicted to affect the compression behavior, resulting in an ~20% increase in the bulk modulus [*Tsuchiya et al.*, 2005]. While a powder X-ray diffraction study has reported evidence for such an anomaly [*Hushur et al.*, 2011], a more recent high-resolution single-crystal X-ray study to 65 GPa found no evidence for a bulk modulus anomaly to at least this pressure [*Rosa et al.*, 2013]. No evidence for hydrogen bond symmetrization was found in an infrared spectroscopic study [*Shieh et al.*, 2009] or in other theoretical calculations [*Mainprice et al.*, 2007]. However, a spin-pairing transition in Fe^{3+}-bearing phase D is reported to produce a pronounced softening of the bulk modulus [*Chang et al.*, 2013].

6.8.2. δ-AlOOH and Phase H

Hydrous aluminum oxides and silicates, such as δ-AlOOH and phase H, are also candidate deep-mantle water carriers. δ-AlOOH is a high-pressure polymorph of diaspore that was initially synthesized at 21 GPa and 1300 K [*Suzuki et al.*, 2000]. Experiments have now shown that its stability extends over the entire range of conditions (to 134 GPa and 2300 K) expected in the lower mantle [*Sano et al.*, 2004, 2008]. At low pressures, δ-AlOOH crystallizes in a distorted rutile-type structure with the noncentrosymmetric orthorhombic space group $P2_1nm$ [*Suzuki et al.*, 2000; *Komatsu et al.*, 2006; *Vanpeteghem et al.*, 2007]. The structure contains both AlO_6 and HO_6 octahedra, and the oxygen anions form a slightly distorted hexagonal close-packed arrangement perpendicular to the *b* direction.

A recent single-crystal X-ray diffraction study indicates that δ-AlOOH transforms to the $CaCl_2$-type structure (space group *Pnnm*) at ~8 GPa [*Kuribayashi et al.*, 2013]. As described above, this structure consists of corner-sharing chains of edge-sharing octahedra (AlO_6, in this case). There is no discontinuity in unit cell volume across this displasive transition. The main difference between the two structures lies in the disordering of hydrogen atoms in the high-pressure structure. The substitution of small amounts of Mg^{2+} and Si^{4+} into δ-AlOOH also promotes the transformation from $P2_1nm$ to the *Pnnm* $CaCl_2$-type structure [*Komatsu et al.*, 2011]. The nature of the hydrogen bonding in these phases has been

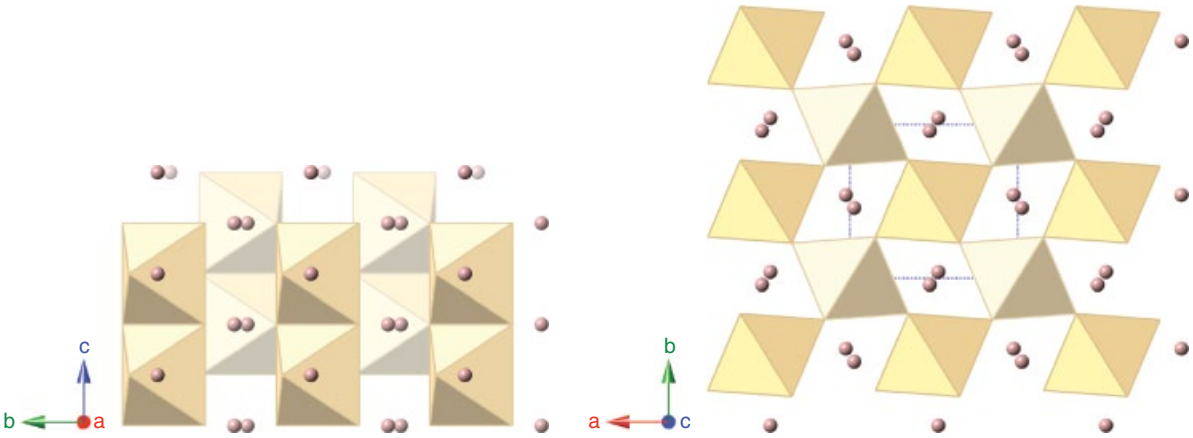

Figure 6.11 View of the phase H structure (space group *Pnnm*, Table 6.3) along the *a* (left) and *c* axis (right). Distorted Mg/Si octahedra (yellow) are charge compensated by H^+ ions (pink spheres), which may occupy one of two positions depicted between the octahedra.

extensively discussed, especially with regard to the formation of symmetric hydrogen bonds, but there is currently no consensus on this issue [*Tsuchiya et al.*, 2002; *Panero and Stixrude*, 2004; *Li et al.*, 2006b; *Xue et al.*, 2006; *Vanpeteghem et al.*, 2007; *Sano-Furukawa et al.*, 2008].

A related hydrous silicate, called phase H, $MgSiO_2(OH)_2$, was predicted theoretically and synthesized near 50 GPa [*Tsuchiya*, 2013; *Nishi et al.*, 2014]. The phase, which contains 15 wt.% water, can be quenched to ambient conditions [*Nishi et al.*, 2014]. A single-crystal X-ray diffraction study on a recovered sample of phase H shows that it adopts the orthorhombic $CaCl_2$-type structure (*Pnnm*), with Mg^{2+} and Si^{4+} disordered over the octahedral sites [*Bindi et al.*, 2014]. H^- positions are expected to be disordered in this structure (Figure 6.11).

The stability field for end-member phase H appears to be relatively narrow and confined to conditions of the upper part of the lower mantle [*Tsuchiya*, 2013; *Ohtani et al.*, 2014]. However, based on structural similarity, it is expected that phase H and δ-AlOOH (whose formulas can be written, respectively, as $MgSiH_2O_4$ and $AlAlH_2O_4$) will exhibit extensive solid solution at high pressures [*Bindi et al.*, 2014]. Experiments have now shown that intermediate δ-AlOOH-$MgSiO_2(OH)_2$ compositions can be synthesized together with perovskite and post-perovskite under slab geotherm conditions, making them plausible candidate hydrous phases under lower mantle conditions [*Ohira et al.*, 2014].

6.9. SUMMARY

In this review, we have summarized the current status of our understanding of lower mantle minerals and their structures. Despite much activity over the last two decades, the lower mantle remains a region that is still poorly understood. Future progress is likely to come from technical advances in high-pressure crystallography. For example, single-crystal synchrotron X-ray diffraction techniques in the diamond anvil cell are now extending into the lower mantle pressure range [*Merlini and Hanfland*, 2013; *Zhang et al.*, 2013; *Duffy*, 2014], and capabilities for simultaneous high *P* and *T* single-crystal diffraction are being pioneered [*Dubrovinsky et al.*, 2010]. These advances will allow us to better understand the crystallographic consequences of cation substitution, water incorporation, and effects of temperature on minerals stable only at these high pressures.

The pressure range of multianvil press techniques can now reach well into the lower mantle range as a result of the development of sintered diamond anvil technology [*Yamazaki et al.*, 2014]. The combined larger sample size and more uniform heating at high pressures may resolve current discrepancies in phase stability and element partitioning between lower mantle phases. Concurrently, the capabilities of theoretical studies using density functional theory have continued to expand [*Wentzcovitch et al.*, 2010]. Each of these developments holds considerable future promise for further understanding of deep-mantle crystal structures in the coming years.

REFERENCES

Adams, D. J., and A. R. Oganov (2006), *Ab initio* molecular dynamics study of $CaSiO_3$ perovskite at P-T conditions of Earth's lower mantle, *Phys. Rev. B*, *73*(18), 184, 106, doi:10.1103/PhysRevB.73.184106.

Akber-Knutson, S., and M. S. T. Bukowinski (2004), The energetics of aluminum solubility into $MgSiO_3$ perovskite at lower mantle conditions, *Earth Planet. Sci. Lett.*, *220*(3–4), 317–330, doi:10.1016/S0012-821X(04)00065-2.

Ammann, M. W., J. P. Brodholt, J. Wookey, and D. P. Dobson (2010), First-principles constraints on diffusion in lower-mantle minerals and a weak D″ layer, *Nature*, *465*(7297), 462–465, doi:10.1038/nature09052.

Ammann, M. W., A. M. Walker, S. Stackhouse, J. Wookey, A. M. Forte, J. P. Brodholt, and D. P. Dobson (2014), Variation of thermal conductivity and heat flux at the Earth's core mantle boundary, *Earth Planet. Sci. Lett*., *390*, 175–185, doi:10.1016/j.epsl.2014.01.009.

Andrault, D., G. Fiquet, F. Guyot, and M. Hanfland (1998), Pressure-induced Landau-type transition in stishovite, *Science*, *282*(5389), 720–724, doi:10.1126/science.282.5389.720.

Andrault, D., N. Bolfan-Casanova, M. A. Bouhifd, N. Guignot, and T. Kawamoto (2007), The role of Al-defects on the equation of state of Al–(Mg,Fe)SiO_3 perovskite, *Earth Planet. Sci. Lett.*, *263*(3–4), 167–179, doi:10.1016/j.epsl.2007.08.012.

Andrault, D., R. G. Trønnes, Z. Konôpková, W. Morgenroth, H. P. Liermann, G. Morard, and M. Mezouar (2014), Phase diagram and P-V-T equation of state of Al-bearing seifertite at lowermost mantle conditions, *Am. Mineral.*, *99*(10), 2035–2042, doi:10.2138/am-2014-4697.

Armstrong, L. S., M. J. Walter, J. R. Tuff, O. T. Lord, A. R. Lennie, A. K. Kleppe, and S. M. Clark (2012), Perovskite phase relations in the system CaO–MgO–TiO_2–SiO_2 and implications for deep mantle lithologies, *J. Petrol.*, *53*(3), 611–635, doi:10.1093/petrology/egr073.

Asahara, Y., K. Hirose, Y. Ohishi, N. Hirao, H. Ozawa, and M. Murakami (2013), Acoustic velocity measurements for stishovite across the post-stishovite phase transition under deviatoric stress: Implications for the seismic features of subducting slabs in the mid-mantle, *Am. Mineral.*, *98*(11–12), 2053–2062, doi:10.2138/am.2013.4145.

Auzende, A.-L., J. Badro, F. J. Ryerson, P. K. Weber, S. J. Fallon, A. Addad, J. Siebert, and G. Fiquet (2008), Element partitioning between magnesium silicate perovskite and ferropericlase: New insights into bulk lower-mantle geochemistry, *Earth Planet. Sci. Lett.*, *269*(1–2), 164–174, doi:10.1016/j.epsl.2008.02.001.

Badro, J. (2014), Spin transitions in mantle minerals, *Annu. Rev. Earth Planet. Sci.*, *42*(1), 231–248, doi:10.1146/annurev-earth-042711-105304.

Badro, J., G. Fiquet, F. Guyot, J.-P. Rueff, V. V. Struzhkin, G. Vankó, and G. Monaco (2003), Iron partitioning in Earth's mantle: Toward a deep lower mantle discontinuity, *Science*, *300*(5620), 789–791, doi:10.1126/science.1081311.

Belonoshko, A. B., L. S. Dubrovinsky, and N. A. Dubrovinsky (1996), A new high-pressure silica phase obtained by molecular dynamics, *Am. Mineral.*, *81*, 785–788, doi:10.2138/am-1996-5-632.

Bindi, L., M. Nishi, J. Tsuchiya, and T. Irifune (2014), Crystal chemistry of dense hydrous magnesium silicates: The structure of phase H, $MgSiH_2O_4$, synthesized at 45 GPa and 1000°C, *Am. Mineral.*, *99*(8–9), 1802–1805, doi:10.2138/am.2014.4994.

Bolfan-Casanova, N., D. Andrault, E. Amiguet, and N. Guignot (2009), Equation of state and post-stishovite transformation of Al-bearing silica up to 100 GPa and 3000 K, *Phys. Earth Planet. Inter.*, *174*(1–4), 70–77, doi:10.1016/j.pepi.2008.06.024.

Bower, D. J., M. Gurnis, J. M. Jackson, and W. Sturhahn (2009), Enhanced convection and fast plumes in the lower mantle induced by the spin transition in ferropericlase, *Geophys. Res. Lett.*, *36*(10), L10,306, doi:10.1029/2009GL037706.

Brodholt, J. P. (2000), Pressure-induced changes in the compression mechanism of aluminous perovskite in the Earth's mantle, *Nature*, *407*(6804), 620–622, doi:10.1038/35036565.

Buffett, B. A., and C. T. Seagle (2010), Stratification of the top of the core due to chemical interactions with the mantle, *J. Geophys. Res. Solid Earth*, *115*(B4), B04,407, doi:10.1029/2009JB006751.

Caracas, R., and R. M. Wentzcovitch (2006), Theoretical determination of the structures of $CaSiO_3$ perovskites, *Acta Crystallogr.*, *B62*, 1025–1030, doi:10.1107/S0108768106035762.

Caracas, R., R. Wentzcovitch, G. D. Price, and J. Brodholt (2005), $CaSiO_3$ perovskite at lower mantle pressures, *Geophys. Res. Lett.*, *32*(6), L06,306, doi:10.1029/2004GL022144.

Catalli, K., S.-H. Shim, V. B. Prakapenka, J. Zhao, W. Sturhahn, P. Chow, Y. Xiao, H. Liu, H. Cynn, and W. J. Evans (2010), Spin state of ferric iron in $MgSiO_3$ perovskite and its effect on elastic properties, *Earth Planet. Sci. Lett.*, *289*(1–2), 68–75, doi:10.1016/j.epsl.2009.10.029.

Chang, Y.-Y., et al. (2013), Spin transition of Fe^{3+} in Al-bearing phase D: An alternative explanation for small-scale seismic scatterers in the mid-lower mantle, *Earth Planet. Sci. Lett*., *382*, 1–9, doi:10.1016/j.epsl.2013.08.038.

Chao, E. C. T., J. J. Fahey, J. Littler, and D. J. Milton (1962), Stishovite, SiO_2, a very high pressure new mineral from Meteor Crater, Arizona, *J. Geophys. Res.*, *67*(1), 419–421, doi:10.1029/JZ067i001p00419.

Cohen, R. E. (1987), Calculation of elasticity and high pressure instabilities in corundum and stishovite with the Potential Induced Breathing Model, *Geophys. Res. Lett.*, *14*(1), 37–40, doi:10.1029/GL014i001p00037.

Cohen, R. E. (1992), First-principles predictions of elasticity and phase transitions in high pressure SiO_2 and geophysical implications, in *High-Pressure Research: Application to Earth and Planetary Sciences*, edited by Y. Syono and M. Manghnani, pp. 425–431, AGU, Washington, D.C.

Dera, P., C. T. Prewitt, N. Z. Boctor, and R. J. Hemley (2002), Characterization of a high-pressure phase of silica from the Martian meteorite Shergotty, *Am. Mineral.*, *87*(7), 1018–1023, doi: 10.2138/am-2002-0728.

Dobson, D. P., N. Miyajima, F. Nestola, M. Alvaro, N. Casati, C. Liebske, I. G. Wood, and A. M. Walker (2013), Strong inheritance of texture between perovskite and post-perovskite in the D″ layer, *Nat. Geosci.*, *6*(7), 575–578, doi:10.1038/ngeo1844.

Dorfman, S. M., S. R. Shieh, Y. Meng, V. B. Prakapenka, and T. S. Duffy (2012), Synthesis and equation of state of perovskites in the $(Mg, Fe)_3Al_2Si_3O_{12}$ system to 177 GPa, *Earth Planet. Sci. Lett*., *357–358*, 194–202, doi:10.1016/j.epsl.2012.09.024.

Dorfman, S. M., Y. Meng, V. B. Prakapenka, and T. S. Duffy (2013), Effects of Feenrichment on the equation of state and stability of (Mg,Fe)SiO_3 perovskite, *Earth Planet. Sci. Lett*., *361*, 249–257, doi:10.1016/j.epsl.2012.10.033.

Dubrovinsky, L., et al. (2010), Single-crystal X-ray diffraction at megabar pressures and temperatures of thousands of degrees, *High Press. Res.*, *30*(4), 620–633, doi:10.1080/08957959.2010.534092.

Dubrovinsky, L. S., S. K. Saxena, P. Lazor, R. Ahuja, O. Eriksson, J. M. Wills, and B. Johansson (1997), Experimental

and theoretical identification of a new high-pressure phase of silica, *Nature*, *388*(6640), 362–365, doi:10.1038/41066.

Dubrovinsky, L. S., N. A. Dubrovinskaia, S. K. Saxena, H. Annersten, E. Hålenius, H. Harryson, F. Tutti, S. Rekhi, and T. L. Bihan (2000), Stability of ferropericlase in the lower mantle, *Science*, *289*(5478), 430–432, doi:10.1126/science.289.5478.430.

Dubrovinsky, L. S., N. A. Dubrovinskaia, S. K. Saxena, F. Tutti, S. Rekhi, T. Le Bihan, G. Shen, and J. Hu (2001), Pressure-induced transformations of cristobalite, *Chem. Phys. Lett.*, *333*(3–4), 264–270, doi:10.1016/S0009-2614(00)01147-7.

Duffy, T. (2014), Crystallography's journey to the deep Earth, *Nature*, *506*(7489), 427–429, doi:10.1038/506427a.

Duffy, T. S. (2005), Synchrotron facilities and the study of the Earth's deep interior, *Rep. Prog. Phys.*, *68*(8), 1811, doi:10.1088/0034-4885/68/8/R03.

Duffy, T. S., R. J. Hemley, and H. Mao (1995), Equation of state and shear strength at multimegabar pressures: Magnesium oxide to 227 GPa, *Phys. Rev. Lett.*, *74*(8), 1371–1374, doi:10.1103/PhysRevLett.74.1371.

Fei, Y., and H. Mao (1994), In situ determination of the NiAs phase of FeO at high pressure and temperature, *Science*, *266*(5191), 1678–1680, doi:10.1126/science.266.5191.1678.

Finkelstein, G., P. Dera, S. Jahn, A. R. Oganov, C. M. Holl, Y. Meng, and T. S. Duffy (2014), Phase transitions and equation of state of forsterite to 90 GPa from single-crystal X-ray diffraction and molecular modeling, *Am. Mineral.*, *99*(1), 35–43, doi:10.2138/am.2014.4526.

Fiquet, G., A. Dewaele, D. Andrault, M. Kunz, and T. Le Bihan (2000), Thermoelastic properties and crystal structure of $MgSiO_3$ perovskite at lower mantle pressure and temperature conditions, *Geophys. Res. Lett.*, *27*(1), 21–24, doi:10.1029/1999GL008397.

Fischer, R. A., A. J. Campbell, O. T. Lord, G. A. Shofner, P. Dera, and V. B. Prakapenka (2011), Phase transition and metallization of FeO at high pressures and temperatures, *Geophys. Res. Lett.*, *38*(24), L24,301, doi:10.1029/2011GL049800.

Frost, D. J., and Y. Fei (1998), Stability of phase D at high pressure and high temperature, *J. Geophys. Res. Solid Earth*, *103*(B4), 7463–7474, doi:10.1029/98JB00077.

Frost, D. J., and Y. Fei (1999), Static compression of the hydrous magnesium silicate phase D to 30 GPa at room temperature, *Phys. Chem. Minerals*, *26*(5), 415–418, doi:10.1007/s002690050202.

Frost, D. J., and C. A. McCammon (2008), The redox state of Earth's mantle, *Annu. Rev. Earth Planet. Sci.*, *36*(1), 389–420, doi:10.1146/annurev.earth.36.031207.124322.

Frost, D. J., C. Liebske, F. Langenhorst, C. A. McCammon, R. G. Trønnes, and D. C. Rubie (2004), Experimental evidence for the existence of iron-rich metal in the Earth's lower mantle, *Nature*, *428*(6981), 409–412, doi:10.1038/nature02413.

Gasparik, T., A. Tripathi, and J. B. Parise (2000), Structure of a new Al-rich, $[K,Na]_{0.9}[Mg.Fe]_2[Mg,Fe,Al,Si]_6O_{12}$, synthesized at 24 GPa, *Am. Mineral.*, *85*, 613–618, doi:10.2138/am-2000-0426.

Ghosh, S., and M. W. Schmidt (2014), Melting of phase D in the lower mantle and implications for recycling and storage of H_2O in the deep mantle, *Geochim. Cosmochim. Acta*, *145*, 72–88, doi:10.1016/j.gca.2014.06.025.

Goresy, A. E., P. Dera, T. G. Sharp, C. T. Prewitt, M. Chen, L. Dubrovinsky, B. Wopenka, N. Z. Boctor, and R. J. Hemley (2008), Seifertite, a dense orthorhombic polymorph of silica from the Martian meteorites Shergotty and Zagami, *Eur. J. Mineral.*, *20*(4), 523–528, doi:10.1127/0935-1221/2008/0020-1812.

Grocholski, B., S.-H. Shim, and V. B. Prakapenka (2013), Stability, metastability, and elastic properties of a dense silica polymorph, seifertite, *J. Geophys. Res. Solid Earth*, *118*(9), 4745–4757, doi:10.1002/jgrb.50360.

Harte, B., and J. W. Harris (1994), Lower mantle mineral associations preserved in diamonds, *Mineral. Mag.*, *58A*, 384–385.

Hazen, R. M. (1976), Effects of temperature and pressure on the cell dimension and X-ray temperature factors of periclase, *Am. Mineral.*, *61*, 266–271.

Hill, R. J., M. D. Newton, and G. V. Gibbs (1983), A crystal chemical study of stishovite, *J. Solid State Chem.*, *47*(2), 185–200, doi:10.1016/0022-4596(83)90007-5.

Hirose, K., N. Takafuji, N. Sata, and Y. Ohishi (2005), Phase transition and density of subducted MORB crust in the lower mantle, *Earth Planet. Sci. Lett.*, *237*(1–2), 239–251, doi:10.1016/j.epsl.2005.06.035.

Hirose, K., R. Wentzcovitch, D. A. Yuen, and T. Lay (2015), 2.05—Mineralogy of the deep mantle—The post-perovskite phase and its geophysical significance, in *Treatise on Geophysics*, 2nd ed., edited by G. Schubert, pp. 85–115, Elsevier, Oxford.

Horiuchi, H., E. Ito, and D. J. Weidner (1987), Perovskite-type $MgSiO_3$: Single-crystal X-ray diffraction, *Am. Mineral.*, *72*, 357–360.

Hsu, H., K. Umemoto, P. Blaha, and R. M. Wentzcovitch (2010), Spin states and hyperfine interactions of iron in $(Mg,Fe)SiO_3$ perovskite under pressure, *Earth Planet. Sci. Lett.*, *294*(1–2), 19–26, doi:10.1016/j.epsl.2010.02.031.

Hushur, A., M. H. Manghnani, J. R. Smyth, Q. Williams, E. Hellebrand, D. Lonappan, Y. Ye, P. Dera, and D. J. Frost (2011), Hydrogen bond symmetrization and equation of state of phase D, *J. Geophys. Res. Solid Earth*, *116*(B6), B06,203, doi:10.1029/2010JB008087.

Iitaka, T., K. Hirose, K. Kawamura, and M. Murakami (2004), The elasticity of the $MgSiO_3$ post-perovskite phase in the Earth's lowermost mantle, *Nature*, *430*(6998), 442–445, doi:10.1038/nature02702.

Imada, S., K. Hirose, and Y. Ohishi (2011), Stabilities of NAL and Ca-ferrite-type phases on the join $NaAlSiO_4$-$MgAl_2O_4$ at high pressure, *Phys. Chem. Minerals*, *38*(7), 557–560, doi:10.1007/s00269-011-0427-2.

Irifune, T., and A. E. Ringwood (1993), Phase transformations in subducted oceanic crust and buoyancy relationships at depths of 600–800 km in the mantle, *Earth Planet. Sci. Lett.*, *117*(1–2), 101–110, doi:10.1016/0012-821X(93)90120-X.

Irifune, T., and T. Tsuchiya (2015), 2.03—Mineralogy of the Earth—Phase transitions and mineralogy of the lower mantle, in *Treatise on Geophysics*, edited by G. Schubert, pp. 33–60, Elsevier, Oxford.

Irifune, T., K. Fujino, and E. Ohtani (1991), A new high-pressure form of $MgAl_2O_4$, *Nature*, *349*(6308), 409–411, doi:10.1038/349409a0.

Irifune, T., T. Shinmei, C. A. McCammon, N. Miyajima, D. C. Rubie, and D. J. Frost (2010), Iron partitioning and density changes of pyrolite in Earth's lower mantle, *Science*, *327*(5962), 193–195, doi:10.1126/science.1181443.

Ito, E. (2015), 2.10—Multi-anvil cells and high pressure experimental methods, in *Treatise on Geophysics*, 2nd ed., edited by G. Schubert, pp. 233–261, Elsevier, Oxford.

Ito, E., A. Kubo, T. Katsura, M. Akaogi, and T. Fujita (1998), High-pressure transformation of pyrope ($Mg_3Al_2Si_3O_{12}$) in a sintered diamond cubic anvil assembly, *Geophys. Res. Lett.*, *25*(6), 821–824, doi:10.1029/98GL00519.

Jackson, J. M., W. Sturhahn, G. Shen, J. Zhao, M. Y. Hu, D. Errandonea, J. D. Bass, and Y. Fei (2005), A synchrotron Mössbauer spectroscopy study of (Mg,Fe)SiO_3 perovskite up to 120 GPa, *Am. Mineral.*, *90*(1), 199–205, doi:10.2138/am.2005.1633.

Jiang, F., G. D. Gwanmesia, T. I. Dyuzheva, and T. S. Duffy (2009), Elasticity of stishovite and acoustic mode softening under high pressure by Brillouin scattering, *Phys. Earth Planet. Inter.*, *172*(3–4), 235–240, doi:10.1016/j.pepi.2008.09.017.

Joswig, W., T. Stachel, J. W. Harris, W. H. Baur, and G. P. Brey (1999), New Ca-silicate inclusions in diamonds—Tracers from the lower mantle, *Earth Planet. Sci. Lett.*, *173*(1–2), 1–6, doi:10.1016/S0012-821X(99)00210-1.

Jung, D. Y., and A. R. Oganov (2005), *Ab initio* study of the high-pressure behavior of $CaSiO_3$ perovskite, *Phys. Chem. Minerals*, *32*, 146–153, doi:10.1007/s00269-005-0453-z.

Karki, B. B., L. Stixrude, and J. Crain (1997a), Ab initio elasticity of three high-pressure polymorphs of silica, *Geophys. Res. Lett.*, *24*(24), 3269–3272, doi:10.1029/97GL53196.

Karki, B. B., L. Stixrude, S. J. Clark, M. C. Warren, G. J. Ackland, and J. Crain (1997b), Elastic properties of orthorhombic $MgSiO_3$ perovskite at lower mantle pressures, *Am. Mineral.*, *82*(5–6), 635–638.

Kato, C., K. Hirose, T. Komabayashi, H. Ozawa, and Y. Ohishi (2013), NAL phase in K-rich portions of the lower mantle, *Geophys. Res. Lett.*, *40*(19), 5085–5088, doi:10.1002/grl.50966.

Kawai, K., and T. Tsuchiya (2012), Phase stability and elastic properties of the NAL and CF phases in the $NaMg_2Al_5SiO_{12}$ system from first principles, *Am. Mineral.*, *97*(2–3), 305–314, doi:10.2138/am.2012.3915.

Kawai, K., and T. Tsuchiya (2015), Small shear modulus of cubic $CaSiO_3$ perovskite, *Geophys. Res. Lett.*, *42*, doi:10.1002/2015GL063446.

Kawai, K., T. Tsuchiya, J. Tsuchiya, and S. Maruyama (2009), Lost primordial continents, *Gondwana Res.*, *16*(3–4), 581–586, doi:10.1016/j.gr.2009.05.012.

Kawakatsu, H., and F. Niu (1994), Seismic evidence for a 920-km discontinuity in the mantle, *Nature*, *371*(6495), 301–305, doi:10.1038/371301a0.

Kesson, S. E., J. D. Fitz Gerald, J. M. G. Shelley, and R. L. Withers (1995), Phase relations, structure and crystal chemistry of some aluminous silicate perovskites, *Earth Planet. Sci. Lett.*, *134*(1–2), 187–201, doi:10.1016/0012-821X(95)00112-P.

Kesson, S. E., J. D. Fitz Gerald, and J. M. Shelley (1998), Mineralogy and dynamics of a pyrolite lower mantle, *Nature*, *393*(6682), 252–255, doi:10.1038/30466.

Kingma, K. J., R. E. Cohen, R. J. Hemley, and H.-k. Mao (1995), Transformation of stishovite to a denser phase at lower-mantle pressures, *Nature*, *374*(6519), 243–245, doi:10.1038/374243a0.

Kohlstedt, D. L., H. Keppler, and D. C. Rubie (1996), Solubility of water in the α, β and γ phases of $(Mg,Fe)_2SiO_4$, *Contrib. Mineral. Petrol.*, *123*(4), 345–357, doi:10.1007/s004100050161.

Kojitani, H., T. Katsura, and M. Akaogi (2007a), Aluminum substitution mechanisms in perovskite-type $MgSiO_3$: An investigation by Rietveld analysis, *Phys. Chem. Minerals*, *34*(4), 257–267, doi:10.1007/s00269-007-0144-z.

Kojitani, H., R. Hisatomi, and M. Akaogi (2007b), High-pressure phase relations and crystal chemistry of calcium ferrite-type solid solutions in the system $MgAl_2O_4$-Mg_2SiO_4, *Am. Mineral.*, *92*(7), 1112–1118, doi:10.2138/am.2007.2255.

Kojitani, H., T. Iwabuchi, M. Kobayashi, H. Miura, and M. Akaogi (2011), Structure refinement of high-pressure hexagonal aluminous phases $K_{1.00}Mg_{2.00}Al_{4.80}Si_{1.15}O_{12}$ and $Na_{1.04}Mg_{1.88}Al_{4.64}Si_{1.32}O_{12}$, *Am. Mineral.*, *96*(8–9), 1248–1253, doi:10.2138/am.2011.3638.

Komabayashi, T., K. Hirose, N. Sata, Y. Ohishi, and L. S. Dubrovinsky (2007), Phase transition in $CaSiO_3$ perovskite, *Earth Planet. Sci. Lett.*, *260*(3–4), 564–569, doi:10.1016/j.epsl.2007.06.015.

Komabayashi, T., S. Maruyama, and S. Rino (2009), A speculation on the structure of the D″ layer: The growth of anti-crust at the core–mantle boundary through the subduction history of the Earth, *Gondwana Res.*, *15*(3–4), 342–353, doi:10.1016/j.gr.2008.11.006.

Komatsu, K., T. Kuribayashi, A. Sano, E. Ohtani, and Y. Kudoh (2006), Redetermination of the high-pressure modification of AlOOH from single-crystal synchrotron data, *Acta Crystallogr. Sect. E*, *62*(11), i216–i218, doi:10.1107/S160053680603916X.

Komatsu, K., A. Sano-Furukawa, and H. Kagi (2011), Effects of Mg and Si ions on the symmetry of δ-AlOOH, *Phys. Chem. Minerals*, *38*(9), 727–733, doi:10.1007/s00269-011-0445-0.

Kondo, T., E. Ohtani, N. Hirao, T. Yagi, and T. Kikegawa (2004), Phase transitions of (Mg,Fe)O at megabar pressures, *Phys. Earth Planet. Inter.*, *143–144*, 201–213, doi:10.1016/j.pepi.2003.10.008.

Kubo, T., T. Kato, Y. Higo, and K. Funakoshi (2015), Curious kinetic behavior in silica polymorphs solves seifertite puzzle in shocked meteorite, *Sci. Adv.*, *1*(4), e1500075, doi:10.1126/sciadv.1500075.

Kudoh, Y., C. T. Prewitt, L. W. Finger, A. Darovskikh, and E. Ito (1990), Effect of iron on the crystal structure of (Mg,Fe)SiO_3 perovskite, *Geophys. Res. Lett.*, *17*(10), 1481–1484, doi:10.1029/GL017i010p01481.

Kudoh, Y., T. Nagase, H. Mizohata, E. Ohtani, S. Sasaki, and M. Tanaka (1997), Structure and crystal chemistry of Phase G, a new hydrous magnesium silicate synthesized at 22 GPa and 1050°C, *Geophys. Res. Lett.*, *24*(9), 1051–1054, doi:10.1029/97GL00875.

Kurashina, T., K. Hirose, S. Ono, N. Sata, and Y. Ohishi (2004), Phase transition in Al-bearing $CaSiO_3$ perovskite: Implications for seismic discontinuities in the lower mantle, *Phys. Earth Planet. Inter.*, *145*(1–4), 67–74, doi:10.1016/j.pepi.2004.02.005.

Kuribayashi, T., A. Sano-Furukawa, and T. Nagase (2013), Observation of pressure-induced phase transition of δ-AlOOH

by using single-crystal synchrotron X-ray diffraction method, *Phys. Chem. Minerals*, *41*(4), 303–312, doi:10.1007/s00269-013-0649-6.

Lakshtanov, D. L., et al. (2007), The post-stishovite phase transition in hydrous alumina-bearing SiO_2 in the lower mantle of the earth, *Proc. Natl. Acad. Sci.*, *104*(34), 13,588–13,590, doi:10.1073/pnas.0706113104.

Li, L., D. J. Weidner, J. Brodholt, D. Alfè, G. D. Price, R. Caracas, and R. Wentzcovitch (2006a), Phase stability of $CaSiO_3$ perovskite at high pressure and temperature: Insights from ab initio molecular dynamics, *Phys. Earth Planet. Inter.*, *155*(3–4), 260–268, doi:10.1016/j.pepi.2005.12.007.

Li, S., R. Ahuja, and B. Johansson (2006b), The elastic and optical properties of the high-pressure hydrous phase δ-AlOOH, *Solid State Commun.*, *137*(1–2), 101–106, doi:10.1016/j.ssc.2005.08.031.

Lin, J.-F., D. L. Heinz, H. Mao, R. J. Hemley, J. M. Devine, J. Li, and G. Shen (2003), Stability of magnesiowüstite in Earth's lower mantle, *Proc. Natl. Acad. Sci.*, *100*(8), 4405–4408, doi:10.1073/pnas.252782399.

Lin, J.-F., S. Speziale, Z. Mao, and H. Marquardt (2013), Effects of the electronic spin transitions of iron in lower mantle minerals: Implications for deep mantle geophysics and geochemistry, *Rev. Geophys.*, *51*(2), 244–275, doi:10.1002/rog.20010.

Lin, Y., R. E. Cohen, S. Stackhouse, K. P. Driver, B. Militzer, L. Shulenburger, and J. Kim (2014), Equations of state and stability of $MgSiO_3$ perovskite and post-perovskite phases from quantum Monte Carlo simulations, *Phys. Rev. B*, *90*(18), 184,103, doi:10.1103/PhysRevB.90.184103.

Liu, L. (1975), Post-oxide phases of forsterite and enstatite, *Geophys. Res. Lett.*, *2*(10), 417–419, doi:10.1029/GL002i010p00417.

Liu, L. (1977), High pressure $NaAlSiO_4$: The first silicate calcium ferrite isotype, *Geophys. Res. Lett.*, *4*(5), 183–186, doi:10.1029/GL004i005p00183.

Liu, L.-g. (1986), Phase transformations in serpentine at high pressures and temperatures and implications for subducting lithosphere, *Phys. Earth Planet. Inter.*, *42*(4), 255–262, doi:10.1016/0031-9201(86)90028-2.

Liu, L.-g., and A. E. Ringwood (1975), Synthesis of a perovskite-type polymorph of $CaSiO_3$, *Earth Planet. Sci. Lett.*, *28*(2), 209–211, doi:10.1016/0012-821X(75)90229-0.

Mainprice, D., Y. Le Page, J. Rodgers, and P. Jouanna (2007), Predicted elastic properties of the hydrous D phase at mantle pressures: Implications for the anisotropy of subducted slabs near 670-km discontinuity and in the lower mantle, *Earth Planet. Sci. Lett.*, *259*(3–4), 283–296, doi:10.1016/j.epsl.2007.04.053.

Manga, M., and R. Jeanloz (1996), Implications of a metal-bearing chemical boundary layer in D″ for mantle dynamics, *Geophys. Res. Lett.*, *23*(22), 3091–3094, doi:10.1029/96GL03021.

Mao, H.-k., J. Shu, Y. Fei, J. Hu, and R. J. Hemley (1996), The wüstite enigma, *Phys. Earth Planet. Inter.*, *96*(2–3), 135–145, doi:10.1016/0031-9201(96)03146-9.

Mao, H.-k., G. Shen, and R. J. Hemley (1997), Multivariable dependence of Fe-Mg partitioning in the lower mantle, *Science*, *278*(5346), 2098–2100, doi:10.1126/science.278.5346.2098.

Mao, H.-k., and W. L. Mao (2007), 2.09—Theory and practice—Diamond-anvil cells and probes for high P–T mineral physics studies, in *Treatise on Geophysics*, edited by G. Schubert, pp. 231–267, Elsevier, Amsterdam.

Mao, H.-k., L. C. Chen, R. J. Hemley, A. P. Jephcoat, Y. Wu, and W. A. Bassett (1989), Stability and equation of state of $CaSiO_3$-perovskite to 134 GPa, *J. Geophys. Res. Solid Earth*, *94*(B12), 17,889–17,894, doi:10.1029/JB094iB12p17889.

Marquardt, H., S. Speziale, H. J. Reichmann, D. J. Frost, F. R. Schilling, and E. J. Garnero (2009), Elastic shear anisotropy of ferropericlase in Earth's lower mantle, *Science*, *324*(5924), 224–226, doi:10.1126/science.1169365.

McCammon, C., J. Peyronneau, and J.-P. Poirier (1998), Low ferric iron content of (Mg,Fe)O at high pressures and temperatures, *Geophys. Res. Lett.*, *25*(10), 1589–1592.

Merkel, S., A. K. McNamara, A. Kubo, S. Speziale, L. Miyagi, Y. Meng, T. S. Duffy, and H.-R. Wenk (2007), Deformation of $(Mg,Fe)SiO_3$ post-perovskite and D" anisotropy, *Science*, *316*(5832), 1729–1732, doi:10.1126/science.1140609.

Merlini, M., and M. Hanfland (2013), Single-crystal diffraction at megabar conditions by synchrotron radiation, *High Press. Res.*, *33*(3), 511–522, doi:10.1080/08957959.2013.831088.

Miura, H., Y. Hamada, T. Suzuki, M. Akaogi, N. Miyajima, and K. Fujino (2000), Crystal structure of $CaMg_2Al_6O_{12}$, a new Al-rich high pressure form, *Am. Mineral.*, *85*(11–12), 1799–1803.

Miyagi, L., W. Kanitpanyacharoen, P. Kaercher, K. K. M. Lee, and H.-R. Wenk (2010), Slip systems in $MgSiO_3$ post-perovskite: Implications for D″ anisotropy, *Science*, *329*(5999), 1639–1641, doi:10.1126/science.1192465.

Miyajima, N., T. Yagi, K. Hirose, T. Kondo, K. Fujino, and H. Miura (2001), Potential host phase of aluminum and potassium in the Earth's lower mantle, *Am. Mineral.*, *86*, 740–746.

Mookherjee, M., B. B. Karki, L. Stixrude, and C. Lithgow-Bertelloni (2012), Energetics, equation of state, and elasticity of NAL phase: Potential host for alkali and aluminum in the lower mantle, *Geophys. Res. Lett.*, *39*(19), L19,306, doi:10.1029/2012GL053682.

Murakami, M., K. Hirose, S. Ono, and Y. Ohishi (2003), Stability of $CaCl_2$-type and α-PbO_2-type SiO_2 at high pressure and temperature determined by in-situ X-ray measurements, *Geophys. Res. Lett.*, *30*(5), 1207, doi:10.1029/2002GL016722.

Murakami, M., K. Hirose, S. Ono, T. Tsuchiya, M. Isshiki, and T. Watanuki (2004a), High pressure and high temperature phase transitions of FeO, *Phys. Earth Planet. Inter.*, *146*(1–2), 273–282, doi:10.1016/j.pepi.2003.06.011.

Murakami, M., K. Hirose, K. Kawamura, N. Sata, and Y. Ohishi (2004b), Post-perovskite phase transition in $MgSiO_3$, *Science*, *304*(5672), 855–858, doi:10.1126/science.1095932.

Nishi, M., T. Irifune, J. Tsuchiya, Y. Tange, Y. Nishihara, K. Fujino, and Y. Higo (2014), Stability of hydrous silicate at high pressures and water transport to the deep lower mantle, *Nat. Geosci.*, *7*(3), 224–227, doi:10.1038/ngeo2074.

Noguchi, M., T. Komabayashi, K. Hirose, and Y. Ohishi (2012), High-temperature compression experiments of $CaSiO_3$ perovskite to lowermost mantle conditions and

its thermal equation of state, *Phys. Chem. Minerals*, *40*(1), 81–91, doi:10.1007/s00269-012-0549-1.

Nomura, R., K. Hirose, N. Sata, and Y. Ohishi (2010), Precise determination of post-stishovite phase transition boundary and implications for seismic heterogeneities in the mid-lower mantle, *Phys. Earth Planet. Inter.*, *183*(1–2), 104–109, doi:10.1016/j.pepi.2010.08.004.

Oganov, A. R., and S. Ono (2004), Theoretical and experimental evidence for a post-perovskite phase of $MgSiO_3$ in Earth's D" layer, *Nature*, *430*(6998), 445–448, doi:10.1038/nature02701.

Oganov, A. R., R. Martoňák, A. Laio, P. Raiteri, and M. Parrinello (2005), Anisotropy of Earth's D" layer and stacking faults in the $MgSiO_3$ post-perovskite phase, *Nature*, *438*(7071), 1142–1144, doi:10.1038/nature04439.

Ohira, I., E. Ohtani, T. Sakai, M. Miyahara, N. Hirao, Y. Ohishi, and M. Nishijima (2014), Stability of a hydrous δ-phase, $AlOOH–MgSiO_2(OH)_2$, and a mechanism for water transport into the base of lower mantle, *Earth Planet. Sci. Lett.*, *401*, 12–17, doi:10.1016/j.epsl.2014.05.059.

Ohta, K., K. Fujino, Y. Kuwayama, T. Kondo, K. Shimizu, and Y. Ohishi (2014), Highly conductive iron-rich (Mg,Fe)O magnesiowüstite and its stability in the Earth's lower mantle, *J. Geophys. Res. Solid Earth*, *119*(6), 4656–4665, doi:10.1002/2014JB010972.

Ohtani, E., Y. Amaike, S. Kamada, T. Sakamaki, and N. Hirao (2014), Stability of hydrous phase H $MgSiO_4H_2$ under lower mantle conditions, *Geophys. Res. Lett.*, *41*(23), 8283–8287, doi:10.1002/2014GL061690.

Ono, S., E. Ito, and T. Katsura (2001), Mineralogy of subducted basaltic crust (MORB) from 25 to 37 GPa, and chemical heterogeneity of the lower mantle, *Earth Planet. Sci. Lett.*, *190*(1–2), 57–63, doi:10.1016/S0012-821X(01)00375-2.

Ono, S., K. Hirose, M. Murakami, and M. Isshiki (2002), Post-stishovite phase boundary in SiO_2 determined by in situ X-ray observations, *Earth Planet. Sci. Lett.*, *197*(3–4), 187–192, doi:10.1016/S0012-821X(02)00479-X.

Ono, S., Y. Ohishi, and K. Mibe (2004), Phase transition of Ca-perovskite and stability of Al-bearing Mg-perovskite in the lower mantle, *Am. Mineral.*, *89*(10), 1480–1485, doi:10.2138/am-2004-1016.

Pamato, M. G., A. Kurnosov, T. B. Ballaran, D. M. Trots, R. Caracas, and D. J. Frost (2014), Hexagonal $Na_{0.41}[Na_{0.125}Mg_{0.79}Al_{0.085}]_2[Al_{0.79}Si_{0.21}]_6O_{12}$ (NAL phase): Crystal structure refinement and elasticity, *Am. Mineral.*, *99*(8-9), 1562–1569, doi:10.2138/am.2014.4755.

Pamato, M. G., R. Myhill, T. Boffa Ballaran, D. J. Frost, F. Heidelbach, and N. Miyajima (2015), Lower-mantle water reservoir implied by the extreme stability of a hydrous aluminosilicate, *Nat. Geosci.*, *8*(1), 75–79, doi:10.1038/ngeo2306.

Panero, W. R., and L. P. Stixrude (2004), Hydrogen incorporation in stishovite at high pressure and symmetric hydrogen bonding in δ-AlOOH, *Earth Planet. Sci. Lett.*, *221*(1–4), 421–431, doi:10.1016/S0012-821X(04)00100-1.

Pearson, D. G., et al. (2014), Hydrous mantle transition zone indicated by ringwoodite included within diamond, *Nature*, *507*(7491), 221–224, doi:10.1038/nature13080.

Prewitt, C. T., and J. B. Parise (2000), Hydrous phases and hydrogen bonding at high pressure, *Rev. Mineral. Geochem.*, *41*(1), 309–333, doi:10.2138/rmg.2000.41.11.

Reid, A. F., and A. E. Ringwood (1969), Newly observed high pressure transformations in Mn_3O_4, $CaAl_2O_4$, and $ZrSiO_4$, *Earth Planet. Sci. Lett.*, *6*(3), 205–208, doi:10.1016/0012-821X(69)90091-0.

Ricolleau, A., J.-P. Perrillat, G. Fiquet, I. Daniel, J. Matas, A. Addad, N. Menguy, H. Cardon, M. Mezouar, and N. Guignot (2010), Phase relations and equation of state of a natural MORB: Implications for the density profile of subducted oceanic crust in the Earth's lower mantle, *J. Geophys. Res. Solid Earth*, *115*(B8), B08202, doi:10.1029/2009JB006709.

Ringwood, A. E. (1975), *Composition and Petrology of the Earth's Mantle*, McGraw-Hill, New York.

Rosa, A. D., M. Mezouar, G. Garbarino, P. Bouvier, S. Ghosh, A. Rohrbach, and C. Sanchez-Valle (2013), Single-crystal equation of state of phase D to lower mantle pressures and the effect of hydration on the buoyancy of deep subducted slabs, *J. Geophys. Res. Solid Earth*, *118*(12), 6124–6133, doi:10.1002/2013JB010060.

Ross, N. L., J. Shu, and R. M. Hazen (1990), High-pressure crystal chemistry of stishovite, *Am. Mineral.*, *75*(7–8), 739–747.

Sakai, T., E. Ohtani, H. Terasaki, N. Sawada, Y. Kobayashi, M. Miyahara, M. Nishijima, N. Hirao, Y. Ohishi, and T. Kikegawa (2009), Fe-Mg partitioning between perovskite and ferropericlase in the lower mantle, *Am. Mineral.*, *94*(7), 921–925, doi:10.2138/am.2009.3123.

Sano, A., E. Ohtani, T. Kubo, and K. Funakoshi (2004), In situ X-ray observation of decomposition of hydrous aluminum silicate $AlSiO_3OH$ and aluminum oxide hydroxide d-AlOOH at high pressure and temperature, *J. Phys. Chem. Solids*, *65*(8–9), 1547–1554, doi:10.1016/j.jpcs.2003.12.015.

Sano, A., E. Ohtani, T. Kondo, N. Hirao, T. Sakai, N. Sata, Y. Ohishi, and T. Kikegawa (2008), Aluminous hydrous mineral δ-AlOOH as a carrier of hydrogen into the core-mantle boundary, *Geophys. Res. Lett.*, *35*(3), L03,303, doi:10.1029/2007GL031718.

Sano-Furukawa, A., K. Komatsu, C. B. Vanpeteghem, and E. Ohtani (2008), Neutron diffraction study of δ-AlOOD at high pressure and its implication for symmetrization of the hydrogen bond, *Am. Mineral.*, *93*(10), 1558–1567, doi:10.2138/am.2008.2849.

Seagle, C. T., D. L. Heinz, A. J. Campbell, V. B. Prakapenka, and S. T. Wanless (2008), Melting and thermal expansion in the Fe–FeO system at high pressure, *Earth Planet. Sci. Lett.*, *265*(3–4), 655–665, doi:10.1016/j.epsl.2007.11.004.

Sharp, T. G., A. E. Goresy, B. Wopenka, and M. Chen (1999), A post-stishovite SiO_2 polymorph in the meteorite Shergotty: Implications for impact events, *Science*, *284*(5419), 1511–1513, doi:10.1126/science.284.5419.1511.

Shen, G., and Y. Wang (2014), High-pressure apparatus integrated with synchrotron radiation, *Rev. Mineral. Geochem.*, *78*(1), 745–777, doi:10.2138/rmg.2014.78.18.

Shieh, S. R., H. Mao, R. J. Hemley, and L. C. Ming (1998), Decomposition of phase D in the lower mantle and the fate of dense hydrous silicates in subducting slabs, *Earth Planet. Sci. Lett.*, *159*(1–2), 13–23, doi:10.1016/S0012-821X(98)00062-4.

Shieh, S. R., T. S. Duffy, and G. Shen (2005), X-ray diffraction study of phase stability in SiO_2 at deep mantle conditions,

Earth Planet. Sci. Lett., *235*(1–2), 273–282, doi:10.1016/j.epsl.2005.04.004.

Shieh, S. R., T. S. Duffy, Z. Liu, and E. Ohtani (2009), High-pressure infrared spectroscopy of the dense hydrous magnesium silicates phase D and phase E, *Phys. Earth Planet. Inter.*, *175*(3–4), 106–114, doi:10.1016/j.pepi.2009.02.002.

Shim, S.-H., R. Jeanloz, and T. S. Duffy (2002), Tetragonal structure of $CaSiO_3$ perovskite above 20 GPa, *Geophys. Res. Lett.*, *29*(24), 2166, doi:10.1029/2002GL016148.

Shim, S.-H., K. Catalli, J. Hustoft, A. Kubo, V. B. Prakapenka, W. A. Caldwell, and M. Kunz (2008), Crystal structure and thermoelastic properties of $(Mg_{0.91}Fe_{0.09})SiO_3$ postperovskite up to 135 GPa and 2,700 K, *Proc. Natl. Acad. Sci.*, *105*(21), 7382–7386, doi:10.1073/pnas.0711174105.

Shu, J., H. Mao, J. Hu, Y. Fei, and R. J. Hemley (1998), Single-crystal X-ray diffraction of wüstite to 30 GPa hydrostatic pressure, *Neues Jahrb. Für Mineral. Abh.*, *172*, 309–323.

Sinclair, W., and A. E. Ringwood (1978), Single crystal analysis of the structure of stishovite, *Nature*, *272*(5655), 714–715, doi:10.1038/272714a0.

Smyth, J. R. (1987), β-Mg_2SiO_4: A potential host for water in the mantle? *Am. Mineral.*, *72*, 1051–1055.

Stachel, T., J. W. Harris, G. P. Brey, and W. Joswig (2000), Kankan diamonds (Guinea) II: Lower mantle inclusion parageneses, *Contrib. Mineral. Petrol.*, *140*(1), 16–27, doi:10.1007/s004100000174.

Stebbins, J. F., S. Kroeker, and D. Andrault (2001), The mechanism of solution of aluminum oxide in $MgSiO_3$ perovskite, *Geophys. Res. Lett.*, *28*(4), 615–618, doi:10.1029/2000GL012279.

Stishov, S. M., and N. V. Belov (1962), Crystal structure of a new dense modification of silica SiO_2, *Dokl. Akad. NAUK SSSR*, *143*(4), 951.

Stixrude, L., R. E. Cohen, R. Yu, and H. Krakauer (1996), Prediction of phase transition in $CaSiO_3$ perovskite and implications for lower mantle structure, *Am. Mineral.*, *81*, 1293–1296, doi: 10.2138/am-1996-9-1030.

Sturhahn, W., J. M. Jackson, and J.-F. Lin (2005), The spin state of iron in minerals of Earth's lower mantle, *Geophys. Res. Lett.*, *32*(12), L12,307, doi:10.1029/2005GL022802.

Sugiyama, M., S. Endo, and K. Koto (1987), The crystal structure of stishovite under pressure up to 6 GPa, *Mineral. J.*, *13*(7), 455–466, doi:10.2465/minerj.13.455.

Sun, T., D.-B. Zhang, and R. M. Wentzcovitch (2014), Dynamic stabilization of cubic $CaSiO_3$ perovskite at high temperatures and pressures from *ab initio* molecular dynamics, *Phys. Rev. B*, *89*(9), 094,109, doi:10.1103/PhysRevB.89.094109.

Suzuki, A., E. Ohtani, and T. Kamada (2000), A new hydrous phase δ-AlOOH synthesized at 21 GPa and 1000°C, *Phys. Chem. Minerals*, *27*(10), 689–693, doi:10.1007/s002690000120.

Tamai, H., and T. Yagi (1989), High-pressure and high-temperature phase relations in $CaSiO_3$ and $CaMgSi_2O_6$ and elasticity of perovskite-type $CaSiO_3$, *Phys. Earth Planet. Inter.*, *54*(3–4), 370–377, doi:10.1016/0031-9201(89)90254-9.

Tange, Y., E. Takahashi, Y. Nishihara, K. Funakoshi, and N. Sata (2009), Phase relations in the system MgO-FeO-SiO_2 to 50 GPa and 2000°C: An application of experimental techniques using multianvil apparatus with sintered diamond anvils, *J. Geophys. Res. Solid Earth*, *114*(B2), B02,214, doi:10.1029/2008JB005891.

Teter, D. M., R. J. Hemley, G. Kresse, and J. Hafner (1998), High pressure polymorphism in silica, *Phys. Rev. Lett.*, *80*(10), 2145–2148, doi:10.1103/PhysRevLett.80.2145.

Tschauner, O., B. Kiefer, H. Liu, S. Sinogeikin, M. Somayazulu, and S.-N. Luo (2008), Possible structural polymorphism in Al-bearing magnesiumsilicate post-perovskite, *Am. Mineral.*, *93*, 533–539, doi:10.2138/am.2008.2372.

Tschauner, O., C. Ma, J. R. Beckett, C. Prescher, V. B. Prakapenka, and G. R. Rossman (2014), Discovery of bridgmanite, the most abundant mineral in Earth, in a shocked meteorite, *Science*, *346*(6213), 1100–1102, doi:10.1126/science.1259369.

Tsuchida, Y., and T. Yagi (1989), A new, post-stishovite high-pressure polymorph of silica, *Nature*, *340*(6230), 217–220, doi:10.1038/340217a0.

Tsuchiya, J. (2013), First principles prediction of a new high-pressure phase of dense hydrous magnesium silicates in the lower mantle, *Geophys. Res. Lett.*, *40*(17), 4570–4573, doi:10.1002/grl.50875.

Tsuchiya, J., T. Tsuchiya, S. Tsuneyuki, and T. Yamanaka (2002), First principles calculation of a high-pressure hydrous phase, δ-AlOOH, *Geophys. Res. Lett.*, *29*(19), 1909, doi:10.1029/2002GL015417.

Tsuchiya, J., T. Tsuchiya, and S. Tsuneyuki (2005), First-principles study of hydrogen bond symmetrization of phase D under high pressure, *Am. Mineral.*, *90*(1), 44–49, doi:10.2138/am.2005.1628.

Tsuchiya, T., R. Caracas, and J. Tsuchiya (2004), First principles determination of the phase boundaries of high-pressure polymorphs of silica, *Geophys. Res. Lett.*, *31*(11), L11,610, doi:10.1029/2004GL019649.

Uchida, T., et al. (2009), Non-cubic crystal symmetry of $CaSiO_3$ perovskite up to 18 GPa and 1600 K, *Earth Planet. Sci. Lett.*, *282*(1–4), 268–274, doi:10.1016/j.epsl.2009.03.027.

Vanpeteghem, C. B., A. Sano, K. Komatsu, E. Ohtani, and A. Suzuki (2007), Neutron diffraction study of aluminous hydroxide δ-AlOOD, *Phys. Chem. Minerals*, *34*(9), 657–661, doi:10.1007/s00269-007-0180-8.

Vinnik, L., M. Kato, and H. Kawakatsu (2001), Search for seismic discontinuities in the lower mantle, *Geophys. J. Int.*, *147*(1), 41–56, doi:10.1046/j.1365-246X.2001.00516.x.

Vinnik, L. P., S. I. Oreshin, S. Speziale, and M. Weber (2010), Mid-mantle layering from SKS receiver functions, *Geophys. Res. Lett.*, *37*(24), L24,302, doi:10.1029/2010GL045323.

Walter, M. J., S. C. Kohn, D. Araujo, G. P. Bulanova, C. B. Smith, E. Gaillou, J. Wang, A. Steele, and S. B. Shirey (2011), Deep mantle cycling of oceanic crust: Evidence from diamonds and their mineral inclusions, *Science*, *334*(6052), 54–57, doi:10.1126/science.1209300.

Wang, D., and R. J. Angel (2011), Octahedral tilts, symmetry-adapted displacive modes and polyhedral volume ratios in perovskite structures, *Acta Crystallogr. B*, *67*(4), 302–314, doi:10.1107/S0108768111018313.

Wang, Y., and D. J. Weidner (1994), Thermoelasticity of $CaSiO_3$ perovskite and implications for the lower mantle, *Geophys. Res. Lett.*, *21*(10), 895–898, doi:10.1029/94GL00976.

Weng, K., H.-k. Mao, and P. Bell (1982), Lattice parameters of the perovskite phase in the system $MgSiO_3$–$CaSiO_3$–Al_2O_3, *Year b. Carnegie Instit. Wash*, *81*, 273–277.

Wentzcovitch, R. M., Z. Wu, and P. Carrier (2010), First principles quasiharmonic thermoelasticity of mantle minerals, *Rev. Mineral. Geochem.*, *71*(1), 99–128, doi:10.2138/rmg.2010.71.5.

Wicks, J. K., J. M. Jackson, and W. Sturhahn (2010), Very low sound velocities in iron-rich (Mg,Fe)O: Implications for the core-mantle boundary region, *Geophys. Res. Lett.*, *37*(15), L15,304, doi:10.1029/2010GL043689.

Xue, X., M. Kanzaki, H. Fukui, E. Ito, and T. Hashimoto (2006), Cation order and hydrogen bonding of high-pressure phases in the Al_2O_3-SiO_2-H_2O system: An NMR and Raman study, *Am. Mineral.*, *91*(5-6), 850–861, doi:10.2138/am.2006.2064.

Yamamoto, T., D. A. Yuen, and T. Ebisuzaki (2003), Substitution mechanism of Al ions in $MgSiO_3$ perovskite under high pressure conditions from first-principles calculations, *Earth Planet. Sci. Lett.*, *206*(3–4), 617–625, doi:10.1016/S0012-821X(02)01099-3.

Yamanaka, T., T. Fukuda, and J. Mimaki (2002), Bonding character of SiO_2 stishovite under high pressures up to 30 Gpa, *Phys. Chem. Minerals*, *29*(9), 633–641, doi:10.1007/s00269-002-0257-3.

Yamanaka, T., A. Uchida, and Y. Nakamoto (2008), Structural transition of post-spinel phases $CaMn_2O_4$, $CaFe_2O_4$, and $CaTi_2O_4$ under high pressures up to 80 GPa, *Am. Mineral.*, *93*(11–12), 1874–1881, doi:10.2138/am.2008.2934.

Yamanaka, T., K. Hirose, W. L. Mao, Y. Meng, P. Ganesh, L. Shulenburger, G. Shen, and R. J. Hemley (2012), Crystal structures of $(Mg_{1-x},Fe_x)SiO_3$ postperovskite at high pressures, *Proc. Natl. Acad. Sci.*, *109*(4), 1035–1040, doi:10.1073/pnas.1118076108.

Yamazaki, D., T. Yoshino, H. Ohfuji, J. Ando, and A. Yoneda (2006), Origin of seismic anisotropy in the D″ layer inferred from shear deformation experiments on post-perovskite phase, *Earth Planet. Sci. Lett.*, *252*(3–4), 372–378, doi:10.1016/j.epsl.2006.10.004.

Yamazaki, D., E. Ito, T. Yoshino, N. Tsujino, A. Yoneda, X. Guo, F. Xu, Y. Higo, and K. Funakoshi (2014), Over 1 Mbar generation in the Kawai-type multianvil apparatus and its application to compression of $(Mg_{0.92}Fe_{0.08})SiO_3$ perovskite and stishovite, *Phys. Earth Planet. Inter.*, *228*, 262–267, doi:10.1016/j.pepi.2014.01.013.

Yang, H., C. T. Prewitt, and D. J. Frost (1997), Crystal structure of the dense hydrous magnesium silicate, phase D, *Am. Mineral.*, *82*, 651–654.

Zhang, L., Y. Meng, P. Dera, W. Yang, W. L. Mao, and H.-k. Mao (2013), Single-crystal structure determination of $(Mg,Fe)SiO_3$ postperovskite, *Proc. Natl. Acad. Sci.*, *110*(16), 6292–6295, doi:10.1073/pnas.1304402110.

Zhang, L., et al. (2014), Disproportionation of $(Mg,Fe)SiO_3$ perovskite in Earth's deep lower mantle, *Science*, *344*(6186), 877–882, doi:10.1126/science.1250274.